Environmental effects and seismogenic source characterization of the December 2020 earthquake sequence near Petrinja, Croatia.

S. Baize[1], S. Amoroso[2,3], N. Belić[4], L. Benedetti[5], P. Boncio[2], M. Budić[4], F.R. Cinti[3], M. Henriquet[5], P. Jamšek Rupnik[6], B. Kordić[4], S. Markušić[7], L. Minarelli[3], D. Pantosti[3], S. Pucci[3], M. Špelić[4], A. Testa[2], S. Valkaniotis[8], M. Vukovski[4]

J. Atanackov[6], J. Barbača[4], M. Bavec[6], R. Brajkovič[6], V. Brčić[4], M. Caciagli[3], B. Celarc[6†], R. Civico[3], P.M. De Martini[3], R. Filjak[4], F. Iezzi[2], A. Moulin[5], T. Kurečić[4], M. Métois[9], R. Nappi[3], A. Novak[6,10], M. Novak[6], B. Pace[2], D. Palenik[4], T. Ricci[3]

[1] Institut de Radioprotection et de Sûreté Nucléaire, IRSN/PRP-ENV/SCAN/BERSSIN, 92262 Fontenay-Aux-Roses, France,

[2] University G. d'Annunzio of Chieti - Pescara, Via dei Vestini 31, 66100, Chieti, Italy

[3] Istituto Nazionale di Geofisica e Vulcanologia, Via di Vigna Murata 605, 00143 Rome, Italy

[4] Croatian Geological Survey, Department of Geology, Sachsova 2, Zagreb, 10000, Croatia

[5] University of Aix Marseille, CNRS, IRD, INRAE, CEREGE, Aix-en-Provence, France

[6] Geological Survey of Slovenia, GeoZS, Dimičeva ulica 14, 1000 Ljubljana, Slovenia. [†]Bogomir Celarc deceased after his valuable contribution to this study, during the review process. All the co-authors present their sincere condolences to his family and friends.

[7] University of Zagreb, Faculty of Science, Department of Geophysics, Zagreb, Croatia

[8] Democritus University of Thrace, Department of Civil Engineering, Polytechnic School, 67100 Xanthi, Greece,

[9] University Claude Bernard of Lyon, Laboratoire de Géologie de Lyon (LGLTPE), Campus de La Doua, 69100 Villeurbane, France

[10] University of Ljubljana, Faculty of Natural Sciences and Engineering, Department of Geology, Slovenia

Abbreviated title: Environmental effects of the Petrinja earthquake

Abstract

On 29 December 2020, a shallow earthquake of magnitude Mw 6.4 struck northern Croatia, near the town of Petrinja, more than 24 hours after a strong foreshock (MI 5). We formed a reconnaissance team of European geologists and engineers, from Croatia, Slovenia, France, Italy and Greece, rapidly deployed in the field to map the evidence of coseismic environmental effects. In the epicentral area, we recognized surface deformation, such as tectonic breaks along the earthquake source at the surface, liquefaction features (scattered in the fluvial plains of Kupa, Glina and Sava rivers), and slope failures, both caused by strong motion. Thanks to this concerted, collective and meticulous work, we were able to document and map a clear and unambiguous coseismic surface rupture associated with the main shock. The surface rupture appears discontinuous, consisting of multi-kilometer *en échelon* right stepping sections, along a NW-SE striking fault that we call the Petrinja-Pokupsko Fault (PPKF). The observed deformation features, in terms of kinematics and trace alignments, are consistent with slip on a right lateral fault, in agreement with the focal solution of the main shock. We found mole tracks, displacement on faults affecting natural features (e. g. drainage channels), scarplets, and more frequently breaks of anthropogenic markers (roads, fences). The surface rupture is observed over a length of ~13 km from end-to-end, with a maximum displacement of 38 cm, and an average displacement of ~10 cm. Moreover, the liquefaction extends over an area of nearly 600 km² around the epicenter. Typology of liquefaction features include sand blows, lateral spreading phenomenon along the road and river embankments, as well as sand ejecta of different grain size and matrix. Development of large and long fissures along the fluvial landforms, current or ancient, with massive

ejections of sediments is pervasive. These features are sometimes accompanied by small horizontal displacements. Finally, the environmental effects of the earthquake appear to be reasonably consistent with the usual scaling relationships, in particular the surface faulting. This rupture of the ground occurred on or near traces of a fault that shows clear evidence of Quaternary activity. Further and detailed studies will be carried out to characterize this source and related faults in terms of future large earthquakes potential, for their integration into seismic hazard models.

Keywords: Seismicity and tectonics, Earthquake hazards, Europe

Introduction

The Mw 6.4 Petrinja earthquake on 29 December 2020 is the shallow (~10 km) mainshock of an earthquake sequence in northern Croatia (Fig. 1). It is one of the largest inland earthquake in Europe since the Mw 6.5 2016 earthquake in Central Italy, more than one year after the 26 November 2019 M 6.4 Dürres earthquake in Albania, both in the Central Mediterranean area. As observed for events of similar size (Civico et al., 2018), the Petrinja earthquake produced widespread environmental effects, mostly within the epicentral area. Among them, a NW-SE striking right-lateral surface rupture occurred along a previously mapped fault, consistently with the focal mechanism and the InSAR dataset analysis, which infers a peak slip of 3.50 m at a 3.5 km depth and ~40 cm at the surface (Xiong et al., 2021). This surface rupture is the first one to be documented in the Balkan region since 1967 (Ambraseys and Jackson, 1998). The strong shaking caused widespread and significant liquefaction in the two main valleys of the Kupa and Sava rivers.

The coseismic effects are primarily dependent on the seismogenic source and its relationship with the shallow crust, the superficial layers (regolith, soils), the water content in distinct units, and the ground surface (Quigley et al., 2016). The most common effects are surface faulting, slope failures, liquefaction, uplift and subsidence, that contribute to changes of the landscape depending primarily on the event magnitude, focal depth and fault kinematics, and the level of changes they caused has

been formalized in the so-called Environmental Seismic Intensity scale (Michetti et al., 2007). Large crustal earthquakes (M>6) commonly produce visible surface faulting, and frequently uplift and subsidence, with noticeable exceptions of blind M>6 events (e.g. Pousse-Beltran et al., 2020). The pattern and magnitude of surface faulting are directly related to the seismogenic rupture at depth (slip amount, fault geometry, surface area, depth), and are therefore reliable indicators for its location, size, and kinematics. (e.g., McCalpin, 2009). Other coseismic secondary effects such as ground failure and liquefaction are related to the size and distribution of the earthquake ground motion coupled with specific geologic and geomorphic settings.

A detailed analysis of the coseismic effects is thus crucial for correlating them with the seismogenic fault at depth, in order to define the geometrical, kinematic and slip distribution of the earthquake source, together with the seismological and geodetic datasets. In addition, the mapping and characterization of the environmental effects can contribute to update the empirical relationships between magnitude and faulting expression (e.g. surface rupture length), liquefaction or landsliding (Obermeier, 1996; Wells and Coppersmith, 1994), and the details of surface faulting can be aggregated into databases to improve fault displacement hazard tools (Baize et al., 2020; Sarmiento et al., 2021). Implementation of recent events data offer a unique opportunity to complement existing empirical relationships, in order to estimate the size and location of potential earthquakes in a region, and contribute to seismic hazard analyses. Ground motion and surface faulting (so-called "coseismic primary effects"), as well as seismic landsliding and liquefaction (so-called "secondary effects"), are a threat to infrastructure and buildings and are responsible for casualties and economic losses: characterizing the impact of earthquakes on the environment is critical to further mitigate their potential consequences on human lives and society, and necessary for land-use planning.

Recent worldwide cases demonstrated that rapid and extensive workforce deployment was essential to document, as complete as possible, the surface effects of M>6 earthquakes (DuRoss et al., 2020; Koehler et al., 2021; Villani et al., 2018). After the December 2020 Mw 6.4 earthquake near Petrinja,

the Croatian Geological Survey (HGI) and a European consortium of earthquake geologists and engineers (from France, Italy, Slovenia, and Greece) joined and conducted a prompt and systematic survey of surface effects in a 625 km² area. Despite challenging conditions (weather and snow cover, minefields and Covid-19 pandemic), the so-called EU team developed an efficient transnational cooperation, documenting more than 700 observation points in the field and analyzing their arrangement in space thanks to remote sensing tools. During the survey, we used the existing 1:100,000 geological maps (Pikija, 1987; Šikić, 2014), post-earthquake geomorphological mapping products based on 1:5,000 topographic maps, Sentinel-2 images (unfortunately often cloudy), orthophoto aerial images available online (Croatian State Geodetic Administration: https://geoportal.dgu.hr/wms), as well as InSAR interferograms derived from the Sentinel-1 constellation. Early drone surveys allowed targeting research to areas affected by extended liquefaction and surface rupture. Following the field mapping campaign, a LIDAR dataset of the epicentral area was acquired and used for further geomorphic expressions related to the earthquake environmental effects.

1) The geological environment

Geological and Seismotectonic context

The Mw 6.4 Petrinja earthquake occurred in the junction between the southwest part of the Pannonian basin and the north of the Internal Dinarides. In terms of regional tectono-stratigraphic background, the Petrinja earthquake region is emplaced between the Adria-derived allochthon units of the Dinarides in the west and Europe-derived units of the Pannonian region (and in particular the "Tisza mega-unit") in the east (Schmid et al., 2020). After the Paleogene collision between Adria and Europe, this region was subjected to extension during the Miocene, then followed by a Pliocene-Quaternary compressional phase , creating a complex network of inverted NW-SE normal faults (Tomljenović and Csontos, 2001; Ustaszewski et al., 2010).

In the epicentral region, Neogene and Quaternary deposits from southwestern part of the Pannonian basin overly older rocks (Jurassic, Cretaceous and Paleogene) that are poorly exposed (Pikija, 1987; Šikić, 2014). Miocene deposits are mainly detrital and clastic deposits, from conglomerates to sands and clays. In a general sense, basal layers of Miocene tend to be coarser ("Otnangian") than the upper ones ("Samartian" and "Pontian"). A noticeable horizon of limestones (calcarenites) is included in the Middle Miocene ("Badenian"). Pliocene layers are mainly of lacustrine and fluvial origin (clays, gravels and sands) of the Pannonian basin, unconformably covering older formations. Plio-Quaternary deposits are an undifferentiated continental ensemble found in the hills of the SW margin of the Pannonian basin. Finally, the youngest layers include aeolian loess (Pleistocene) and fluvial to colluvial deposits (Pleistocene to Holocene). Most of the ruptures mapped at the surface were observed in the Badenian (Middle Miocene) limestones and in Pleistocene to Holocene loose sediments.

Geodetic horizontal velocity field (see Figure 1 for an illustration) shows that the region is placed between the northward moving and counter-clockwise rotating Adriatic microplate, on one hand, and the eastward moving European units, on the other hand (Serpelloni et al., 2016; Weber et al., 2010). Long-term (10^4-10^6 years) tectonic signal is in accordance, at first order, with this short-term scheme. For instance, in the northern section of the Dinarides, in Slovenia, geological and geomorphological data suggest recent activity of the NW-SE Dinaric Fault System where large and active faults (e.g. Raša, Idrija, Predjama faults) accommodate most of the convergence between Adria and Europe (Matoš et al., 2014; Moulin et al., 2016; Pavičić et al., 2019; Placer et al., 2010) (Fig. 1). This structural pattern (NW-SE strike-slip faults) is replaced by W-E trending Sava Folds between eastern Slovenia and northeastern Croatia, which gradually transitions to ENE-WSW striking transpressive to compressive faulting around Zagreb (Matoš et al., 2014; Pavičić et al., 2019), due to the influence of a mega shear zone oriented NE-SW in Hungary (so called, Mid-Hungarian Shear Zone) (Atanackov et al., 2021; Tomljenović and Csontos, 2001). South of Zagreb, the region is characterized by NW-SE dextral faults, such as the one that caused the 2020 Petrinja earthquakes,

which are considered active during the Pliocene and Quaternary, and capable to generate large earthquakes (Basili et al., 2013; Matoš et al., 2014; Pavičić et al., 2019).

Currently, most of the geodetically-determined 5 to 6 mm/yr convergence rate (Nocquet, 2012) between Adria and Europe appears to be accommodated within the (coastal) external Dinarides, although a gap of GPS station coverage unfortunately precludes any accurate strain rate estimation in the wider region of the 2020 earthquake sequence (Métois et al., 2015). Based on focal mechanisms, the stress direction oscillates around the N-S axis in most of the Internal Dinarides – Pannonian region (Herak et al., 2009), consistently with the geodesy velocity field (at first order).

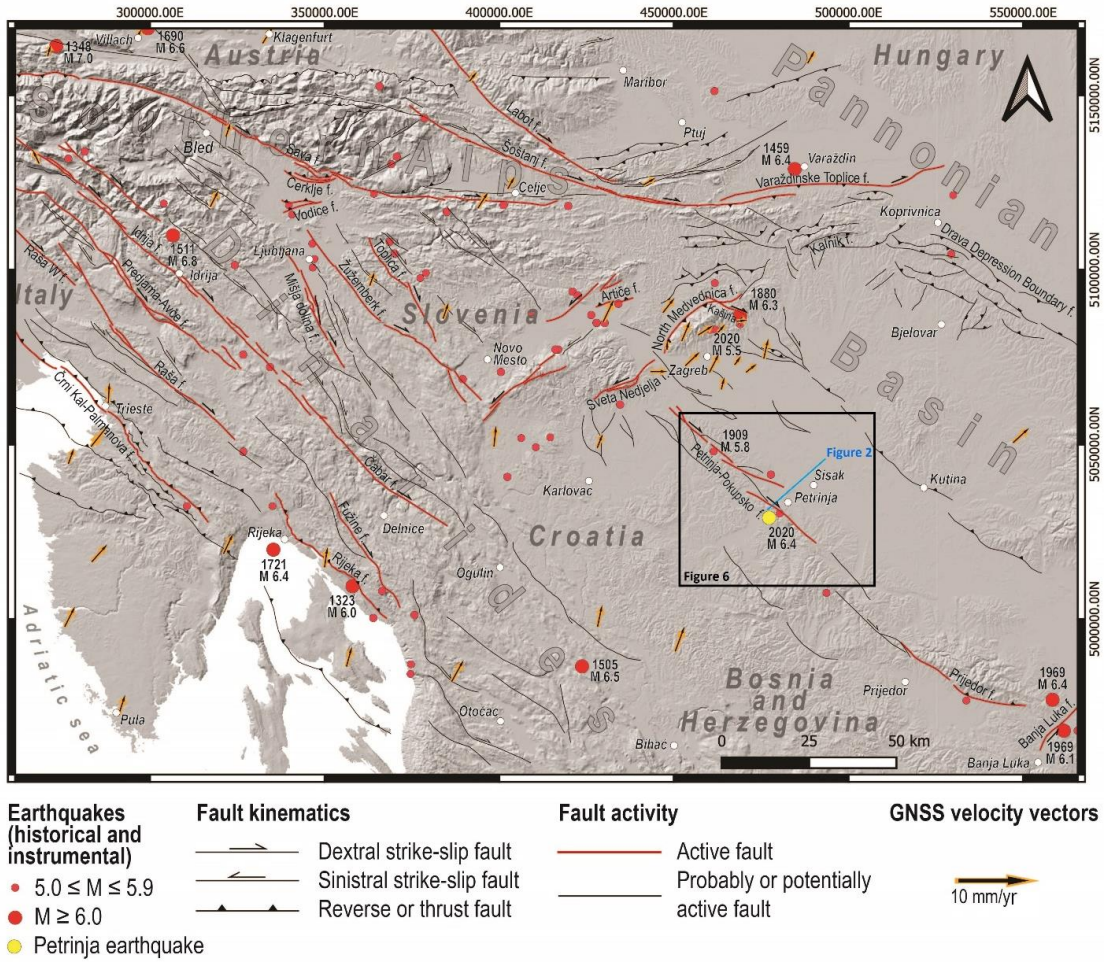

Figure 1. Seismotectonic map of the northern Dinarides and southwestern Pannonian basin. Faults are from Atanackov et al. (2021); Matoš et al. (2014); Tomljenović and Csontos (2001), historical and instrumental earthquakes with magnitudes M ≥ 5 are from SHARE European Earthquake Catalogue (SHEEC)

(Stucchi et al., 2013; Grünthal et al., 2013); shaded relief map produced from Copernicus 25 m resolution Digital Elevation Model, and Global Navigation Satellite Systems (GNSS) field represents horizontal velocities of stations relative to (considered) stable Eurasia (vectors are from Kreemer et al., 2014)

The Internal Dinarides and the Pannonian basin hosted several damaging earthquakes since the beginning of the 20th century (Herak et al., 2009, 1996) (Fig. 1). A strong earthquake shook the region on 17th August 1903 and caused moderate damage in Petrinja with a magnitude estimated to 4.6. The iconic Croatian earthquake occurred on the 8th October 1909 (known as the Pokupsko or Kupa Valley earthquake following Herak and Herak, 2010), with an epicenter located only ~20 km northwest of the 2020 one: the famous Croatian seismologist Andrija Mohorovičić highlighted the boundary between the Earth's crust and the mantle (Moho) after analyzing the seismograms of this earthquake (Mohorovičić, 1992). The epicentral intensity was I_0=VIII MCS with an estimated magnitude between 5.8 and 6.0 and hypocentral depth of around 14 km. The 1909 earthquake focal mechanism, reconstructed from historical seismograms, is consistent with the dextral-transpressive activation of a N140°E, 60° north-east-dipping fault. The mainshock was followed by a series of more than 50 aftershocks until the end of 1910. The strongest one occurred on 29th January 1910 with a magnitude of 5.3. During the last century, the 1969 deadly Banja Luka earthquake (M_L 6.4) happened 100 km to the southeast in Bosnia and Herzegovina (Fig. 1), in a similar location at the transition between the Dinarides and the Pannonian basin (Ustaszewski et al., 2014); the source of this event is unclear, however consistent with a N-S striking maximum horizontal stress. In the last 30 years (before December 2020), the strongest earthquake (M_L 4.5) in the region occurred in 1996 with an epicenter located 3 km south of Petrinja (Herak et al., 2009, 1996).

In the broader region of Central Croatia, the most active area is close to the capital city, Zagreb, about 50 km from the 2020 mainshock epicenter. On the 20th March 2020, the city was shaken by an M_L5.5 earthquake, caused by an ENE-WSW blind reverse fault under the capital city. Severe damage at intensity level I_{max}=VII-VIII MSK was reported (Markušić et al., 2020). In the same area, the national catalogue and the European historical earthquake database (Grünthal et al., 2013; Herak et al., 1996; Stucchi et al., 2013) lists a series of at least 9 significant earthquakes in the Zagreb to Pokupsko area, including the 1880 M~6.0 Zagreb earthquake.

Geological characterization of the PPKF

The Petrinja earthquake shook the NW part of Croatia, with an epicenter located in the vicinity of the NW-SE striking Petrinja composite seismogenic source defined in the EDSF European database (Basili et al., 2013).

This Petrinja composite source of Basili et al. (2013) potentially includes the NW-SE northeast-dipping Pokupsko fault, proposed by Herak and Herak (2010) as the potential source of the large 1909 Kupa Valley earthquake. The Petrinja composite source is, in the European database, a seismogenic source assumed as being multiple structures based on structural and geophysical analysis. It extends over 60 km in length and to about 17 km in depth, and it is dipping 55-70° to the northeast. Its slip rate is not constrained, but Basili et al. (2013) provide a range of 0.08 to 0.2 mm/yr, based on expert judgment. The Petrinja composite source was estimated to be capable of generating earthquakes with a maximum magnitude of 6.5. During the 2020 earthquake sequence, the NW-SE dextral rupture probably involved portions of this composite source, however showing a different geometry with a steep and SW-oriented dip. We define the 2020 earthquake source as the Petrinja-Pokupsko Fault (PPKF), based on its surface trace and deep geometry.

In order to evaluate the fault geometry at depth, we present an analysis of a composite seismic section and interpret the fault zone structure in the vicinity of the hypocenter (ranging between 8 and 13 km, depending on the agency, see Table 1). The composite line comprises original data from three seismic lines recorded for oil and gas exploration during the 1970s and '80s; these lines are available on request at the Croatian Hydrocarbon Agency CHA, as well as well data used for calibration. In this paper, the data have been re-analyzed using the Petrel E&P software platform from Schlumberger. Time-to-depth conversion was performed using velocity data from the Sisak-1 well, from which a two-layer interval velocity model was produced. Two first-order tectonostratigraphic units can be delineated on this line, including the pre-Neogene basement and

Neogene to Quaternary basin fill (Fig. 2). The basin fill can be divided into Lower to Middle Miocene, Upper Miocene, and Pliocene to Quaternary deposits.

The architecture in Figure 2 is a result of a complex tectonic evolution. The Neogene episodes include the syn-rift extension during Lower to Middle Miocene, the post-rift subsidence in basal Upper Miocene, and the positive tectonic inversion since the Uppermost Miocene (Horváth et al., 2006; Tomljenović and Csontos, 2001). This inversion phase activated the PPKF as a deep-seated dextral strike-slip fault zone, as exemplified by the seismic data, which appears clearly as a positive flower structure. The pre-Neogene basement and Neogene-Quaternary basin fill form a wide antiform around the PPKF. The profiles also cleary show the tilting and thickening of Neogene deposits towards the NE and the Sisak-1 well, and the correlated deepening of the pre-Neogene basement interface. The first-order basin structure is controlled by the syn-rift detachment normal faults (in pink on Fig. 2), dipping towards the NE. Their listric geometry is revealed in the hanging wall by rollover anticline structures within the Paleogene horizons and related syncline in the syn-rift horizons (Lower Miocene). Subtle deformation features of the reflectors also reveal the influence of late, inverting and steeply dipping faults. Internal seismic reflector arrangement suggests the timing of tilting and initiation of the PPKF uplift: the basal part of Upper Miocene deposits is dominantly concordant with the Lower to Middle Miocene deposits, whereas the top part of the Upper Miocene deposits unconformably overly the older pack (blue line), with onlapping strata (see between the 7 and 15 km of Fig. 2). This suggests that the PPKF and Hrastovica Mt. zone uplift may then have started in the Upper Miocene.

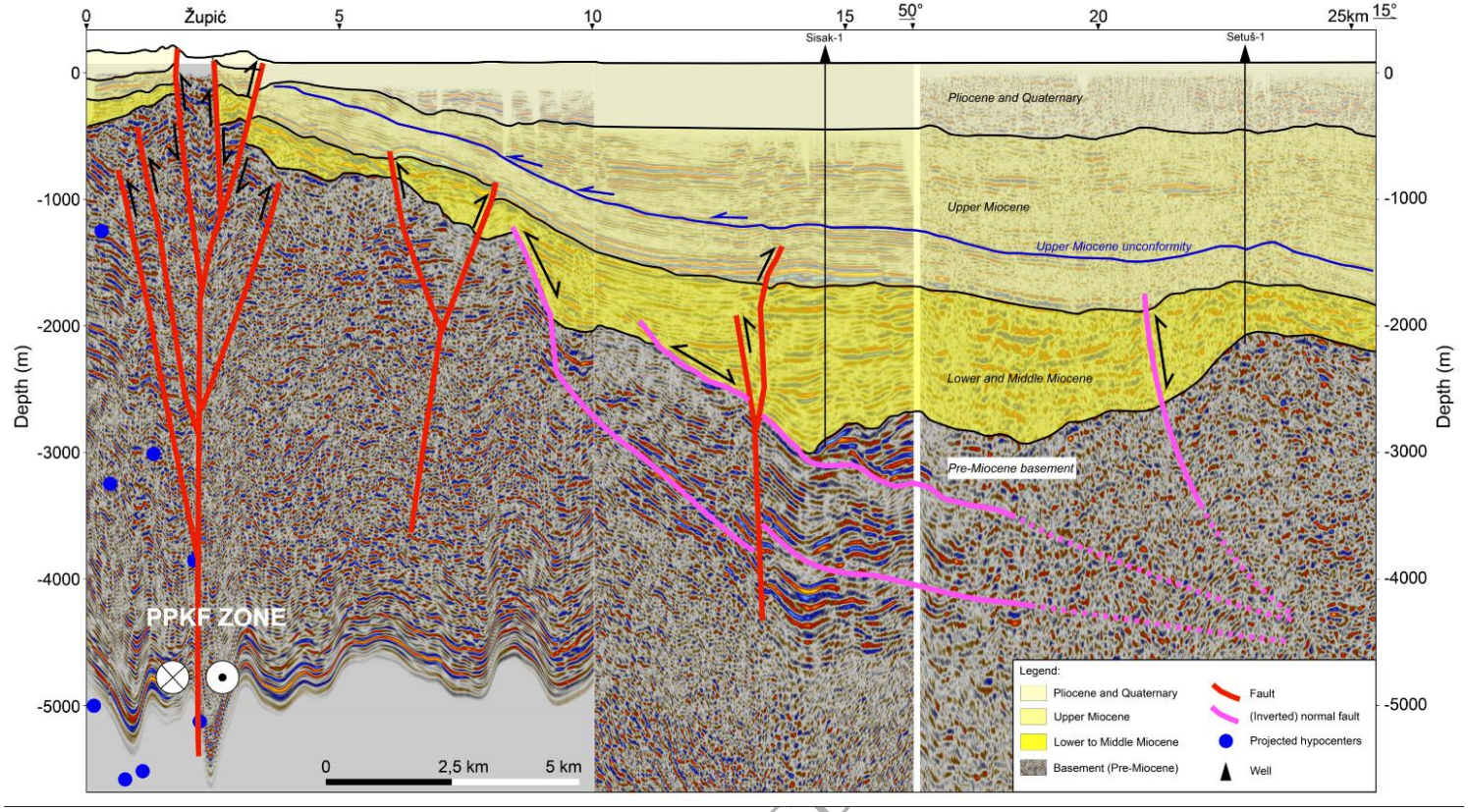

Figure 2. Composite seismic section showing the regional structural and stratigraphic relations of the research area (see Fig. 1 and 3 for location). Vertical exaggeration is 2.5. Seismic lines are available at the Croatian Hydrocarbon Agency CHA (https://www.azu.hr/en). A pristine version is provided in Supplementary Material (S5).

2. The earthquake sequence

2.1. Seismology

The sequence started on 28 December, 2020, in the early morning hours (05:28 UTC), with an M_L5.0 earthquake that caused damage in Petrinja. The epicenter was about 5 km southwest of Petrinja. This event actually saved many human lives, as it forced many inhabitants to immediately move out of their homes before the main shock on 29 December 2020 (M_L6.2), in the late morning (12:19 UTC).

The moment magnitude of the mainshock has been estimated between Mw 6.3 and 6.5 by several agencies, with a hypocentral depth ranging from 7.8 to 13.5 km (Table 1). The Seismological Survey at the Department of Geophysics (Faculty of Science, University of Zagreb) yielded the catalogue of the sequence with earthquake magnitudes in local scale (ML), and more accurate hypocentral depths. This catalogue is based on detection by the Seismological Survey permanent network (https://www.pmf.unizg.hr/geof/seizmoloska_sluzba/) and a specific crustal model described by (Herak et al., 1996). The distribution of the sequence epicenters is shown in Fig. 3a. More information is provided in Supplementary Material (S2).

The mainshock epicenter is located 2 km west of the ML 5 foreshock and only 2 km SW of the main surface trace of the PPKF and related surface ruptures near Župić. The mainshock was followed by 5 significant aftershocks in the 24 hours, with magnitudes ranging from M_L4.6 to 4.8 and depths ranging between 5.8 and 12.2 km. These last events are notably and exclusively located 2.5 to 5 km NW of the mainshock, close to the Međurače rupture section (see hereafter).

The focal mechanisms of the mainshock, provided by the 5 agencies reported in Table 1, are very consistent and put forward a NW-SE sub-vertical to steeply SW dipping rupture plane at shallow depth (8 to 13 km). This is totally consistent with the location of the epicenter in respect to the observed surface rupture (see thereafter), but contradicts the NE dip of the Basili et al. (2013) composite source. A preliminary analysis of seismological recordings from remote stations suggests

that the main shock rupture propagated with a slow velocity, and with a high stress drop - a characteristic of some slowly deforming active faults (Causse, 2021).

Considering the whole sequence, the cluster of epicenters clearly stretches roughly along the PPKF surface trace, mainly on its southwestern side (Fig. 3a). This is consistent with a steep angle of the main source to the SW, as revealed by the main shock focal mechanisms of several agencies (Table 1). The vertical representation of the hypocenter cloud (Fig. 3b) however depicts a nearly vertical structure from the ground surface to the deep part of the crust, which does not support the hypothesis of a reactivation of a former normal and low-angle fault at depth. A cluster of low magnitude aftershocks stands out 5 km NE of the PPKF at depth larger than 6 km, a bit east of Petrinja.

Table 1. Various focal mechanism solutions provided by 6 agencies:

(1) http://cnt.rm.ingv.it/en/event/25870121; (2) http://geofon.gfz-potsdam.de/eqinfo/event.php?id=gfz2020zocb; (3) https://earthquake.usgs.gov/earthquakes/eventpage/us6000d3zh/; (4) http://sismoazur.oca.eu/focal_mechanism_emsc; (5) http://geoscope.ipgp.fr/index.php/en/catalog/earthquake-description?seis=us6000d3zh ;

	Mw	depth (km)	strike (°)	dip (°)	(°)	reference
INGV	6.3	9	128	89	179	(1)
GFZ	6.4	11	131	83 SW	167	(2)
USGS	6.4	13.5	134	76 SW	179	(3)
OCA	6.5	8	130	70 SW	180	(4)
IPGP	6.4	13	133	87	172	(5)
U. Zagreb	6.3	7.8	130	84	168	this study

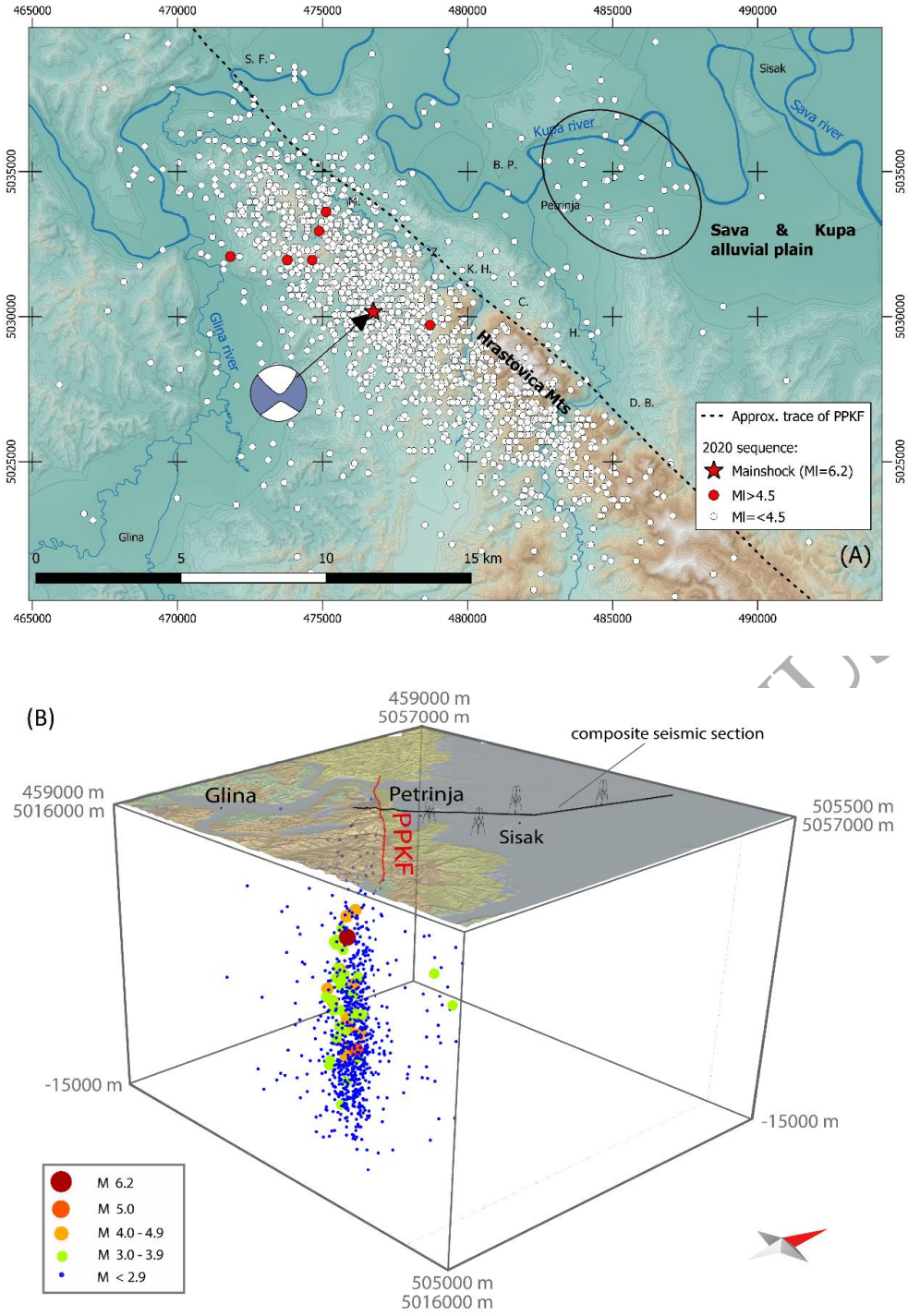

Figure 3. Top) Map distribution of the earthquake epicenters associated with the Petrinja sequence (from 28/12/2020 to 04/01/2021), with epicentral data from the Seismological Survey, Department of Geophysics, Faculty of Science, University of Zagreb; focal mechanism from GFZ. Bottom) Spatial representation of the hypocentres (vertical exaggeration 2.0) regarding the PPKF surface trace (dashed line), composite seismic section (Fig. 2b), and well locations. The ellipse delineates the aftershock swarm (see text, Discussion).

2.2. Geodesy

The Sentinel-1 constellation captured the surface deformation related to the mainshock, as well as the foreshock and the major aftershocks. In Figure 4, we present the ground deformation (horizontal, East-West component) captured by the interferograms between pre- (18th December 2020) and post-earthquake (4th January 2021) Sentinel-1 SAR images. We used ascending 146 track and descending 124 track co-seismic pairs for decomposition into horizontal and vertical displacement components. The InSAR images were processed using ESA SNAP and SNAPHU software. The first order analysis of InSAR signal of the earthquake (wrapped interferograms and Line-of-Sight displacement) promptly yielded the information that surface rupture could have occurred, and partly guided our field survey. However, the coseismic signal is partially blurred in the expected location of the ground breaks: the very low coherence in the near-field fault might be due to the presence of vegetation, unconsolidated deformation and liquefaction. In addition, the same pair of ascending and descending InSAR data allowed the identification of post-seismic deformation, thanks to the images covering the 30th December 2020 to 28th January 2021 time range (Fig. 4b). The coseismic and post-seismic ground deformation patterns are both consistent with a major right-lateral and NW-SE striking surface fault trace. Off-fault ruptures are not distinguishable from the InSAR data. Maximum eastward displacement (red) exceeds ~30 cm on the NE block between the fault zone and Petrinja city, and along a ~7-8 km long section of the fault between Župić (Z.) and Hrastovica (H.) and even Donja Budičina (D. B.), whereas westward displacement is maximal (~30 cm; blue) between Međurače (M.) and Župić (Z.) (Fig. 4a): this defines a relatively sharp 10-15 km long deformation zone at the surface. The post-seismic deformation pattern (Fig. 4b) stretches along the same NW-SE geological structure, however extending slightly to the south of the coseismic signal, beyond Donja Budičina (D. B.), but above all to the north up to Stari Farkašić (S. F.). The complete co- and post-seismic fault trace is punctuated by field-confirmed evidence of surface deformation (see further sections).

Figure 5 shows displacement vectors of geodetic benchmarks, confirming the first-order InSAR signal of a major NW-SE striking right-lateral rupture. Benchmarks were stabilized before the Petrinja earthquake sequence (2003-2020) and were re-measured just after the sequence (8th January 2021-13th March 2021) with a GNSS receiver using the Croatian Positioning Virtual Reference System online service for precise positioning. The accuracy of benchmarks measurements with the aforementioned service is 2 cm in horizontal and 4 cm in vertical direction (Kordić et al., 2019; Pavasović et al., 2016). Considering the time range that is covered, the displacement amount at each site includes the co- and post-seismic displacement (2020 sequence); the fraction of the interseismic tectonic loading might too small to be measurable. The largest values of benchmark displacements are measured close to the center of Petrinja, with 75 centimeters in the ESE direction. In the town of Sisak, planar displacements are around 7 centimeters to the east, while in the town of Glina displacements are around 6 centimeters to the NW. The largest values of NW displacement (65 cm) are measured in Strašnik, close to the epicenter.

Interestingly, the GNSS and InSAR datasets demonstrate that the co- and post-seismic displacements related to the 2020 earthquake sequence are coherent with a right-lateral motion along the NW-SE striking PPKF zone along a ~10-15 km section between Međurače (M.) and Donja Budičina (D. B.). InSAR data suggest that post-seismic deformation could have been concentrated along narrow bands (around 5 cm of afterslip on the Međurače section 1) and that this deformation has extended off the coseismic rupture tips (see labels 1 and 2 on Figure 4b).

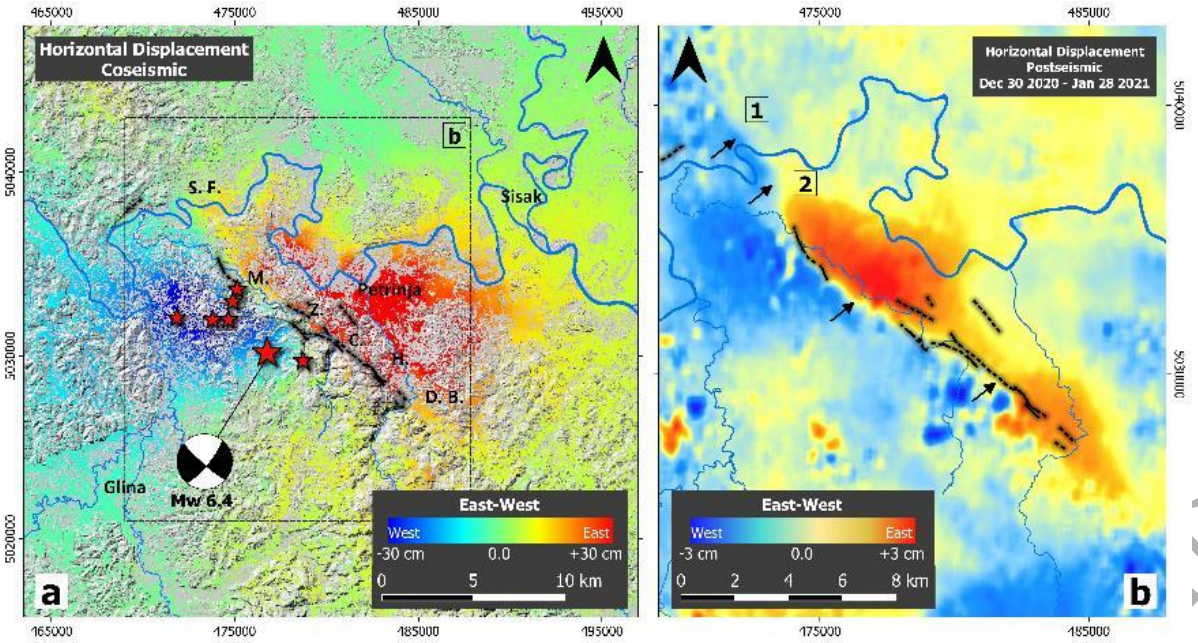

Figure 4. InSAR analysis of the earthquake sequence using Copernicus Sentinel-1 images. a) Horizontal co-seismic displacement (East-West component) from the decomposition of tracks 146 & 124. Focal mechanism from GFZ. b) Horizontal post-seismic displacement (East-West component) from the decomposition of tracks 146 & 124. Post-seismic offset is visible along most of the co-seismic rupture trace length (dashed black line), but also along an additional section (1) where co-seismic rupture was not clearly observed at the surface. This section is connected with the co-seismic rupture through a step (2) where tiny cracks were observed in the field. S. F.: Stari Farkašić, M.: Međurače, Z.: Župić, B. P.: Brest Pokupski, K. H.: Križ Hrastovački, C.: Cepeliš, H.: Hrastovica, D. B.: Donja Budičina. Projection system is HTRS96/Croatia TM, EPSG:32633.

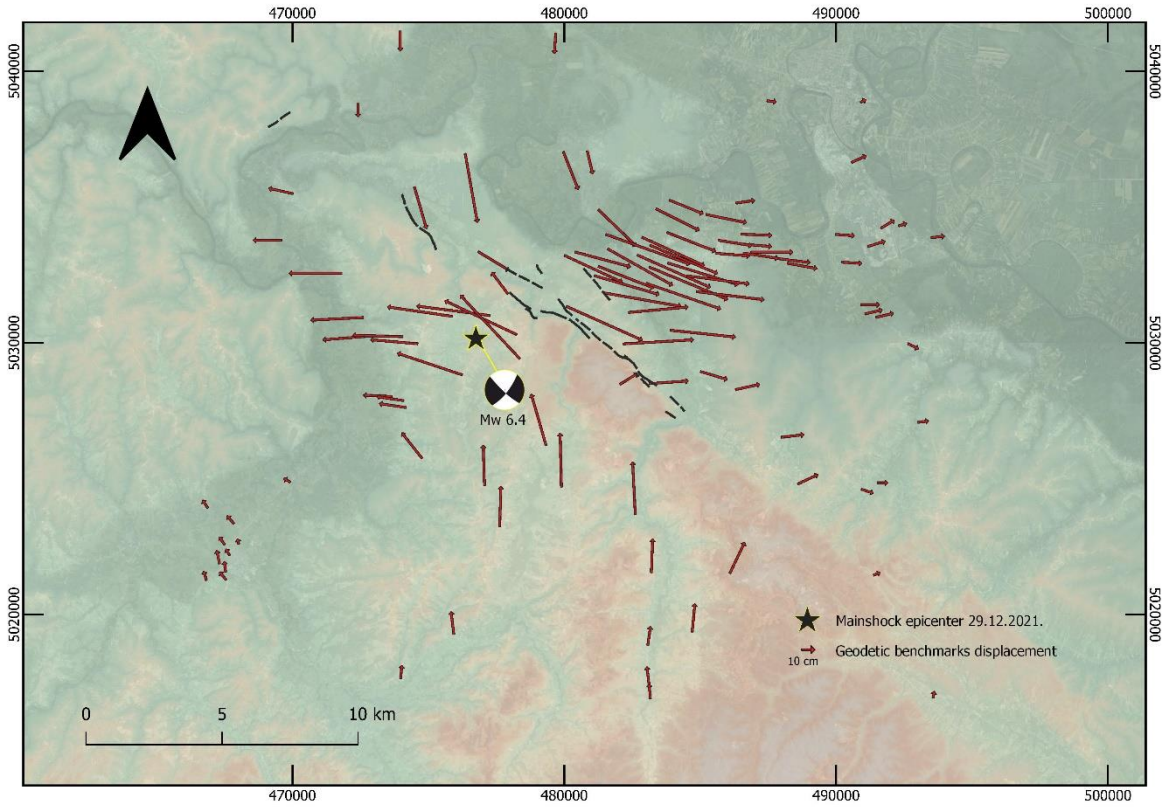

Figure 5. Geodetic benchmarks displacement field after survey covering the earthquake sequence time span, after re-measurement of geodetic benchmarks in 2021. Benchmarks were stabilized before the Petrinja earthquake sequence (2003-2020) and were re-measured just after the sequence (8th January 2021-13th March 2021) with GNSS receiver using Croatian Positioning Virtual Reference System online service for precise positioning. Dashed black line represents the coseismic surface rupture. Main shock location after University of Zagreb catalogue, and focal mechanism after GFZ.

3. Environmental effects

Geologists from Croatia initiated a field survey during the first days after the event, screening the roads and easy-to-drive paths to rapidly cover the area, avoiding the loss of information that could have been erased by repairs, rapid erosion, etc. From 5th January until the 26th March, Slovenian (GeoZS: Geological Survey of Slovenia), French (IRSN: Nuclear Safety Institute, CEREGE: University of Aix-Marseille) and Italian (University of Chieti-Pescara, INGV: Geophysical and Volcanological Institute) geologists joined the Geological Survey of Croatia team (HGI) to proceed with a concerted and cooperative reconnaissance of the coseismic surface effects, together with a remote sensing contribution from colleagues from Greece (U. Thessaloniki). The weather conditions in the

immediate days after the event were challenging for field work, with low temperatures, frequent snow cover, intermittent fog, and periodic showers. This limited the operability of the teams in densely forested slopes and wetlands. In addition, the earthquake area includes several uncleared minefields from the 1991-1995 Croatian War of Independence which precluded any field investigation; some of these areas were covered with drone surveys to image the liquefaction features. The mobilization and work of the team members was further hampered by the COVID-19 pandemic, and required significant beforehand preparation in terms of online coordination meetings, logistical anticipation, definition of protocols and safety measures. Due to the restrictions imposed by the pandemic, the different national teams could never work together in-person in the field. However, we reached an efficient collaborative work thanks to numerous online meetings at each step of the investigation, including the preparation of field surveys, the sharing of available and newly acquired data and materials, the update of recordings, the interpretation of data and the elaboration of the outcomes presented here.

As a whole, more than 700 recordings of deformation features such as coseismic cracking, fissuring or faulting, landsliding and liquefaction phenomenon were logged. Several key locations of surface faulting (numbered as “sites” in the database; Supplementary Material S1.2) were observed and measured several times until March 2021. Those potential different recordings of the same site are reported in the database. Figure 6 presents the location and extension of the environmental effects of the 2020 earthquake, as collected by the EU team. We document 3 types of effects, including slope failures (landslides), liquefaction features, and surface ruptures, with a large focus on the latter two. Massive coseismic sinkholes (up to 20 m wide and 12 m deep) were described after the earthquake in the southern part of the area (Mečenčani). We did not focus on them, and the reader can refer to Pollak et al. (2021) for this specific effect.

The surface ruptures were characterized from field observations in the vicinity of the PPKF within the area of deformation determined from InSAR data. Landslides were mapped in the field within a 20-km radius from the mainshock epicenter and using the InSAR data in a broader area. Liquefactions

were mapped in the field and using remote sensing data, in a 600 km^2 area covering the Kupa, Glina and Sava alluvial plains.

3.1. Surface rupture

The initial survey during the first few days after the mainshock provided a general overview of the surface faulting and cracking pattern, which appeared to be centered on the PPKF. First recognitions highlighted that the asphalt roads around Petrinja city were extensively damaged, mostly by cracks without distinct displacement or with cm-scale openings and offsets, which were later confirmed as clear evidence of right-lateral offsets.

Field surveys collected a structural parameters' set measured with tape and compass. We observed features such as cracks (fractures without relative displacement and without opening larger than 1 cm), fissures (tensional cracks, i.e. fractures with observable opening, without relative displacement), and ruptures due to faulting (fracture with measurable relative displacement larger than 1 cm), or warping. We measured their strike, slip amount (throw, slip along strike, net offset), slip vector, opening and documented with photos. The slip vector azimuth has been measured along preserved striations in mud smears or by matching piercing points on both sides of the ruptures. Measurements of the amount of slip have been collected on the direction of the slip vector azimuth, measuring the relative distance between two piercing points. This type of acquisition is classically applied to characterize surface ruptures (e. g. Villani et al., 2018) and provides reliable information for database implementation (e. g. Baize et al., 2020). This information has been used to build the maps in Figure 7, and it is reported in the core table available in Supplementary material (S1.2).

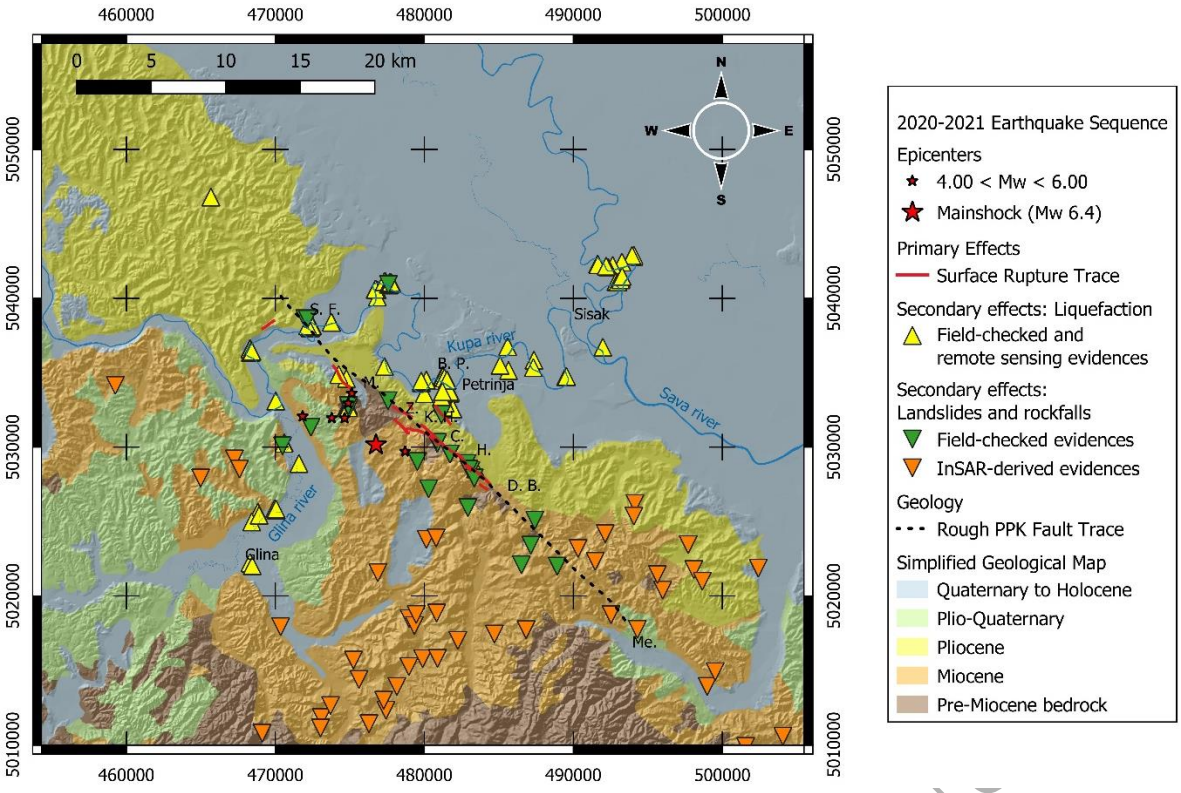

Figure 6. General map of location of the environmental effects caused by the 2020 earthquake sequence of Petrinja. Map shows a rough trace of the PPK fault (black dashed line), the source of the earthquakes, primary effects (surface rupture, in red) as well as secondary effects (liquefaction features and landslides) evidences. Geological map is simplified from Pikija (1987) and Šikić (2014). S. F.: Stari Farkašić, M.: Međurače, Me.: Mečenčani, Z.: Župić, B. P.: Brest Pokupski, K. H.: Križ Hrastovački, C.: Cepeliš, H.: Hrastovica, D. B.: Donja Budičina.

The ruptures affected various types of substratum (Figs 8 to 12, and additional illustrations in Supplementary Material, Figs S1.4.1 to S1.4.6): Quaternary sediments (unconsolidated colluvium and alluvium) in agricultural fields and forests, and Miocene bedrock (weakly consolidated calcarenites), either on or close to the PPKF. When the ruptures propagated through soft-sediments, such as colluvium and alluvium, we measured the slip vector azimuth by matching piercing points on both sides of the rupture, and measured the slip amount along the direction of the slip vector azimuth (Figs 10 and 12). When the ruptures propagated across Miocene-bedrock rocks, we measured the slip vector azimuth and the slip amount along preserved fresh striations in mud smears (e.g. Fig. 8a'). In several cases these ruptures also affected roads, walls and other man-made features. In these cases, we measured the slip vector azimuth and the slip amount by matching evident piercing points

in man-made features (Figs 8a'' and 11). In places, discrete ruptures were sometimes enhanced by far-field bending, increasing the total offset (Figure 11). The crucial observations with measurable surface rupture are all located between Međurače to the NW and Hrastovica to the SE, in the central part of the PPKF, for a total length of ~13 km (Fig. 6 and 7). The rupture trace mostly strikes NW-SE, with evidence of right-lateral slip and localized zones of extension (gravity-drive grabens, opening) or contraction (push-up ridges, mole tracks) at local bends of the rupture trace. For instance, remarkable compressional kinks deformed the asphalt roads near Župić along the fault line (see Figure S1.4.2 in Supplementary Material), which were promptly fixed. Mole tracks were formed at the Kladnjik stream (Fig. 9).

A large part of the surveyed points were cracks on asphalt roads, located off any potential active fault, beyond the maximum deformation area delineated by the InSAR data, and perpendicular to the roads' directions. They are likely related to ground shaking, to decoupling of tar from the underlying soft ground or to bending due to settlement. When associated with tectonic strain, fractures on asphalt are affected by refraction of deformation at the interface tar/ground. Therefore, the features across asphalt covers are poorly informative on the actual occurrence of fault rupture or its strike. On the other hand, meaningful sites on asphalt roads, useful for the reconstruction of the earthquake rupture trace exist too, especially in the vicinity of the PPKF. There, they are characterized by dense fracturing coupled with lateral or vertical relative displacements, with cm-scale offsets on individual ruptures (e.g., "Site 1", Fig. 8a, or "site 6" in the database). Some authors considered some tensional fractures with significant opening and associated liquefaction ejecta of tectonic origin (Markušić et al., 2021; Tondi et al., 2021). Because of their characteristics and location, we do not consider these features as caused by surface faulting, but as liquefaction and lateral-spreading driven features: we describe them in section 3.2.

Taking into consideration the whole dataset of collected observations, we conclude that the 2020 Petrinja earthquake rupture consists of 4 main right-lateral sections (red lines) with a general NW-SE

direction (Figure 7A). These sections also include inferred traces, *i.e.* short strands of punctual observations and ambiguous continuity (dashed lines in Figure 7A). We hereby distinguish the following rupture sections from north to south:

- The **Međurače** section (**section 1** in Fig. 7A), ~2 km long with a maximum net offset of ~0.12 m; it could not be tracked southward across the ~3 km-long observational gap due to minefields (see Supplementary Material S1.1 for their location). An example of evidence of surface faulting in section 1 is illustrated in Supplementary Material (S1.4).
- The **Župić** section (**section 2** in Figure 7A) is separated from the Međurače strand by the observational gap. It is ~1.5 km long with an outstanding offset of the road 37 between Glina and Petrinja (site 1, Fig. 8) and the maximum observed offset (38 cm) (site 5, Fig. 9). It is composed of two right-stepping *en-échelon* segments. A short (1.3 km), low-slip (max. 2 cm) and uncertain rupture was mapped parallel to strand 2 near Župić, based on the alignment of small offsets observed on tar roads.
- The **Križ** section (**section 3** in Fig. 7A) steps to the left to the Župić strand; it is ~2 km long and characterized by the presence of mole tracks in an open field with a left-stepping *en échelon* pattern and 15 cm of right-lateral offset (site 8, Fig. 10). A water pipe was displaced by ~10 cm at the southern tip (site 7), a few hundred meters NW of the tar road tightly chopped by fractures and tiny ruptures (site 6).
- The **Cepeliš** section (**section 4** in Figure 7A) jumps to the Križ strand through a left stepover. It is the most continuous rupture, running over 4.5 km at the toe of the hills and close to the long-term fault. It exhibits right-lateral offsets, such as the ~20 cm offset measured on a wall in Križ (site 9, Fig. 11) or the tiny lateral component visible along the scarplet across colluvial deposits, near Hrastovica (site 10, Fig. 12). Other ruptures, with important vertical component (max. 25 cm), are documented a bit south of site 10 (site 11, Fig. 12), probably because of a significant gravitational component. The southernmost tip of the rupture is

unclear, but can be likely set north of Donja Budičina (D.B.) and the Petrinjčica river outlet in the Petrinja basin.

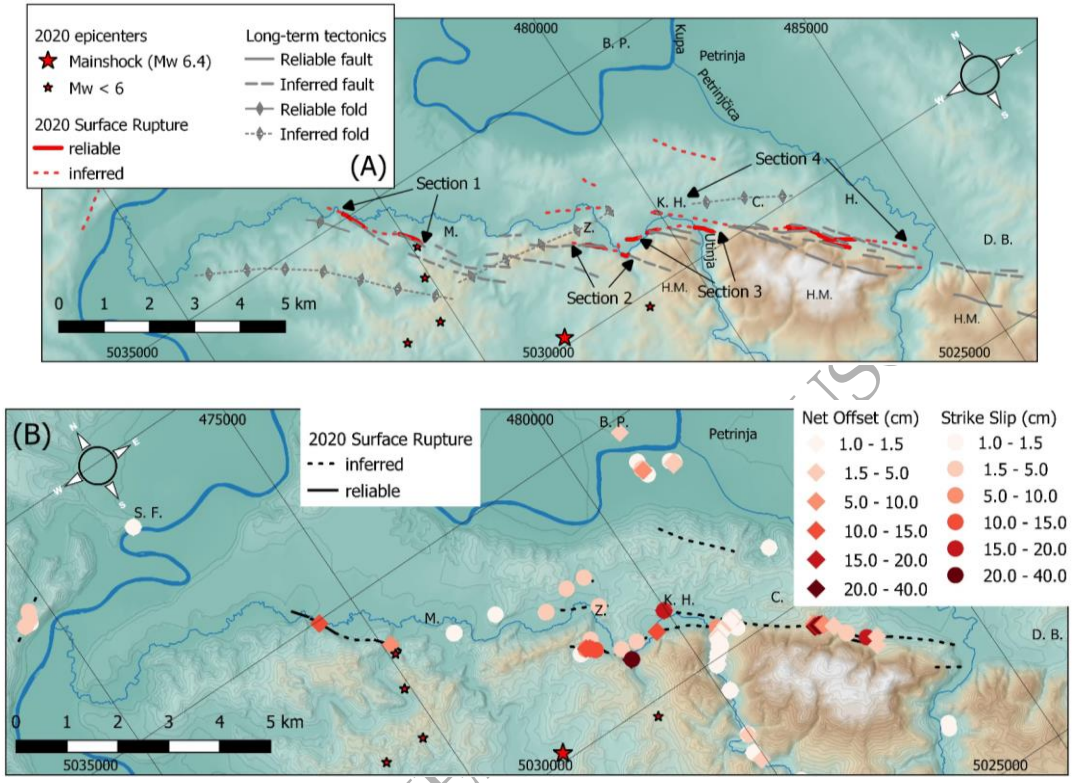

Figure 7: Maps representing the surface rupture, (A) with the sections showing reliable and inferred traces, stars represent the mainshock and main events of the sequence (section 1: Međurače; section 2: Župić ; section 3: Križ; section 4: Cepeliš) and (B) with the offsets measured in the field (B). Notice that the separation between the sections 1 and 2 is due to a lack of observation (mine fields). The database is available in Supplementary Material (S2.1). S. F.: Stari Farkašić, M.: Međurače, Z.: Župić, B. P.: Brest Pokupski, K. H.: Križ Hrastovački, C.: Cepeliš, H.: Hrastovica, H. M.: Hrastovica Mountains, D. B.: Donja Budičina.

All these ruptures are interpreted as evidence of coseismic surface faulting (primary tectonic effects), given their kinematics and structural characteristics, their morphological expressions and their relationships with Quaternary faults. Ruptures occur on flat zones and slopes, crosscutting the morphology or enhancing Quaternary tectonic scarps. In most of cases, gravitational forces cannot be invoked in triggering the observed surface ruptures. Measured right-lateral net displacement varies from a few centimeters to up to 38 cm.

The InSAR data show that the largest displacements along the surface rupture occurred along the sections 2 to 4 during the co-seismic and early post-seismic phase (before January 4th, Fig. 4a), in the range of the field observations (30 cm). Along these sections 2 to 4, the post-seismic offset (December 30th to January 28th) is minimum (<2 cm) relative to the northern parts of the rupture (observation gap and section 1) with up to 5 cm. Notice that we can even infer tiny post-seismic offsets north of section 1 where several cm-scale offsets where locally observed. Notwithstanding this afterslip along section 1, the field measurements (right-lateral offsets of ~10 cm) support the fact that the earthquake surface rupture propagated up to Međurače.

Based on the earthquake rupture mapping and the offset measurements, we propose a rough along-strike slip distribution diagram as representative of the fault rupture that propagated up to the surface from the causative Mw 6.4 Petrinja source at depth (Figs 2 and 3b). In order to display the along-strike slip distribution diagram of the total offset, an aggregate curve is built by summing up the contribution of all the surface faulting sections, in particular in coincidence of overlapping strands (Fig. 13).

Overall, the surface rupture mapping appears discontinuous: this can be an intrinsic characteristic of the earthquake mechanics and/or geological context. This discontinuous character could be a consequence of the (1) moderate earthquake magnitude and slip distribution at depth, (2) shortly-

spaced bedrock tectonic structuration within the PPKF which could control the fragmentation of surface faulting, (3) mechanical characteristics of the shallow geology (i.e. unconsolidated Plio-Quaternary and Holocene sediments such as marsh and alluvial clays capping weakly consolidated to consolidated Badenian calcarenites), possibly causing brittle faulting diffusion and attenuation approaching the surface. These latter surficial geological conditions have abundantly been documented as a major factor controlling surface rupture patterns after recent earthquakes along surface ruptures (e.g. Koehler et al., 2021), and confirmed by analog (sand-box) modelling (e.g. Moss et al., 2018). However, the discontinuous character could also be a consequence of other factors. Adverse weather conditions (e.g. snow cover, heavy rain, frost, etc) affecting the region soon after the event and terrain conditions (e.g., saturated soil, undergrowth, leaves covering the ground), as well as uncleared minefields, hampered the field survey and caused an incomplete collection of surface rupture features.

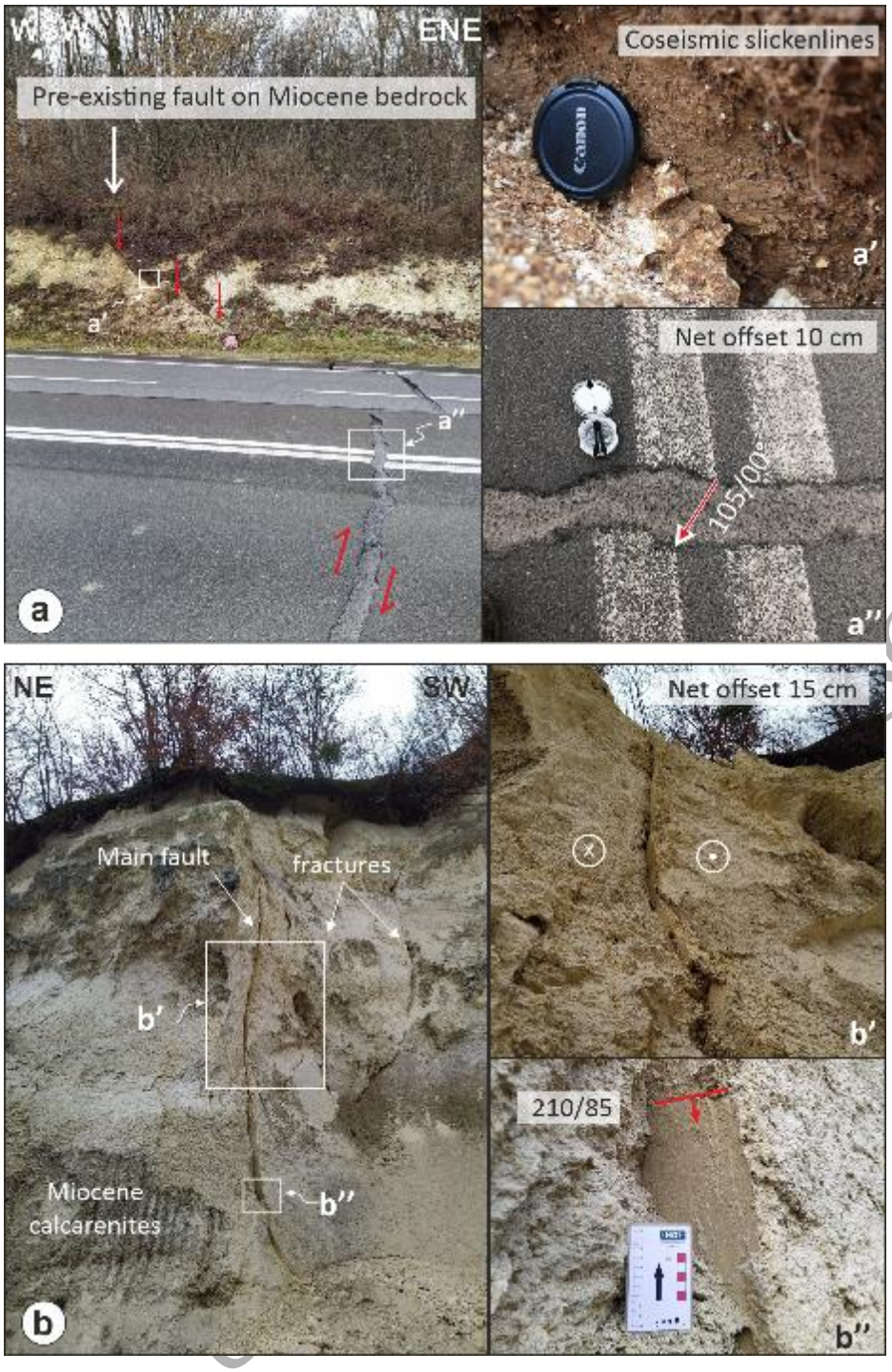

Figure 8: Surface faulting on the Župić section (section 2 in Fig. 7), corresponding to the "Site 1" in database. a): Coseismic rupture is remarkable across the road and the bedrock (Badenian calcarenites); the rupture is diffracted from its original trace in bedrock when reaching the tar road and its embankment. The original opening of the rupture across the road is not visible anymore, as it was rapidly repaired. b) Several hundred meters to the SE, the surface rupture disrupts the wall of a quarry in the Badenian calcarenites.

Figure 9: Surface faulting south of Križ Hrastovački on the Župić section (section 2 on Fig. 7; "site 5" in database). A continuous, approximately 55 m long, coseismic surface rupture zone was observed crossing Kladnjik stream, a tributary of the Utinja River, and the nearby field and dirt road. Coseismic disjunction between a concrete reservoir and a PVC water pipeline transversal to the faulting was reported by locals a few tens of meters west of the surface ruptures (see arrow in main picture A). Ruptures have a left-stepping arrangement with mole tracks (pictures B and C) and a gentle warp of the ground across an approximately 5 m wide zone parallel to the fault. A wide zone of flooding occurs on the left bank of the stream as a consequence of dextral offset (main picture A). The creek shows a cumulative dextral offset up to 2 m. The 2020 coseismic offset can be reconstructed by using singularities in its edges as piercing points: a minimum coseismic lateral motion of 0.3-0.4 m has been estimated. These values are affected by uncertainty in the reconstruction of the original edges that are eroded and presently modified by the mole tracks and because they were surveyed about 2 months after the earthquake.

Figure 10. Aerial view (drone survey) of a ~20 m-long surface rupture on alluvial fan gravels mapped southwest of Križ Hrastovački on the Križ section (section 3 on Fig. 7, "Site 8" in database). Surface faulting occurred as a continuous rupture, striking 120°, or as a set of left-stepping en échelon ruptures. The maximum coseismic offset, measured between well-preserved piercing points, is ~15 cm.

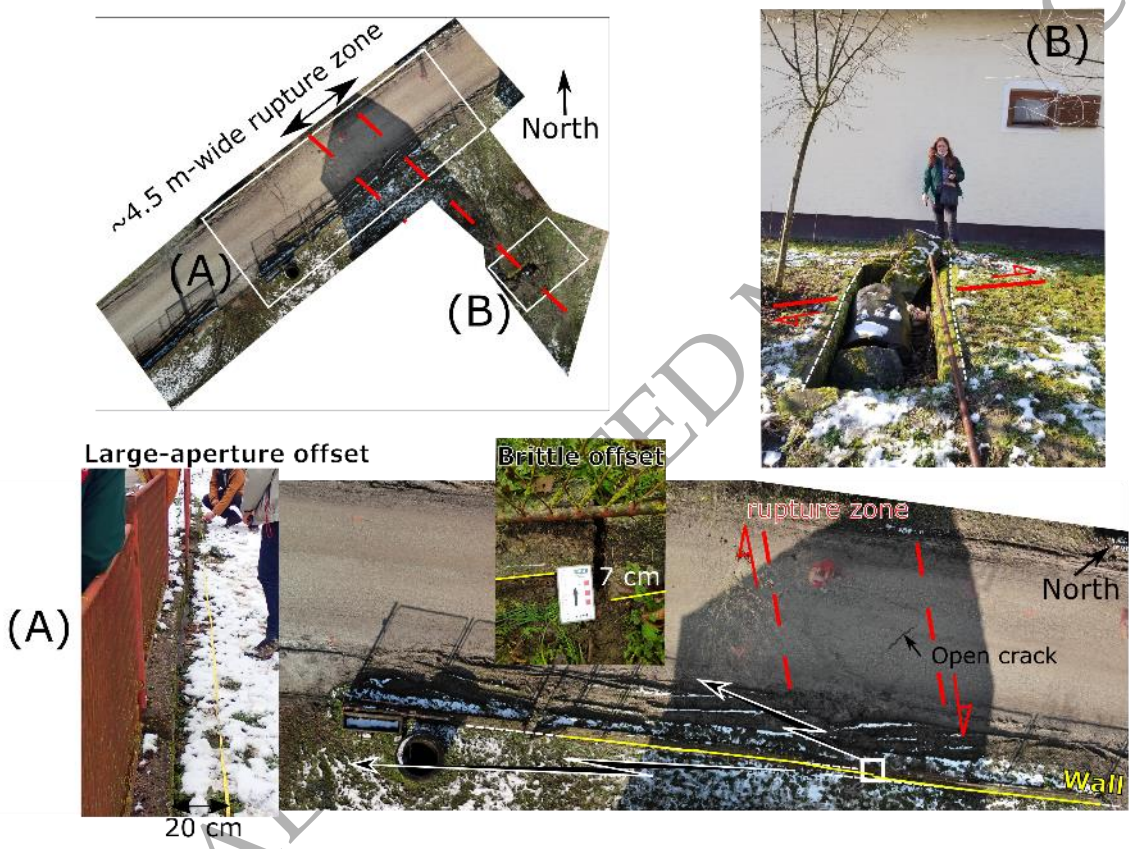

Figure 11. Križ Hrastovački wall site ("Site 9" in database), at the northern tip of the Cepeliš section (section 4 on Fig. 7). The upper left view is a drone photomosaic of the whole site where a ~20 cm right-lateral offset was inferred based on analysis of deformations of man-made features. (A): The brittle and discrete offset of the wall (7 cm) is included in a 4.5 m wide zone within which a ~20 cm large-aperture offset (i.e. total relative displacement across the rupture zone) is accommodated. (B): In the NW-SE continuation of (A), the backyard lawn is bumped and potentially distorted a concrete pit; offset from the pit cannot be estimated as the projection line of the walls is too short.

Figure 12. Surface faulting along the southern portion of the Cepeliš section (section 4 on Fig. 7) (sites 9 and 10). a) Centimetric vertical component of the displacement affecting colluvial deposits. b) Detail of the piercing points along the rupture pattern used to assess the slip vector for net offset measurements with right-lateral transtensional kinematics. c) En-échelon arrangement with a large overlapping step over and enhanced vertical component due to the contribution of the gravitational instability in the slope. d) and e) Dominant decimetric vertical displacements with centimetric right-lateral motion affecting Quaternary alluvial deposits. f) Tensional component of the displacement (open crack), locally resulting in a gravity graben, due to the contribution of slope instability. A detailed map of those sites is provided in Supplementary Material (S1.4).

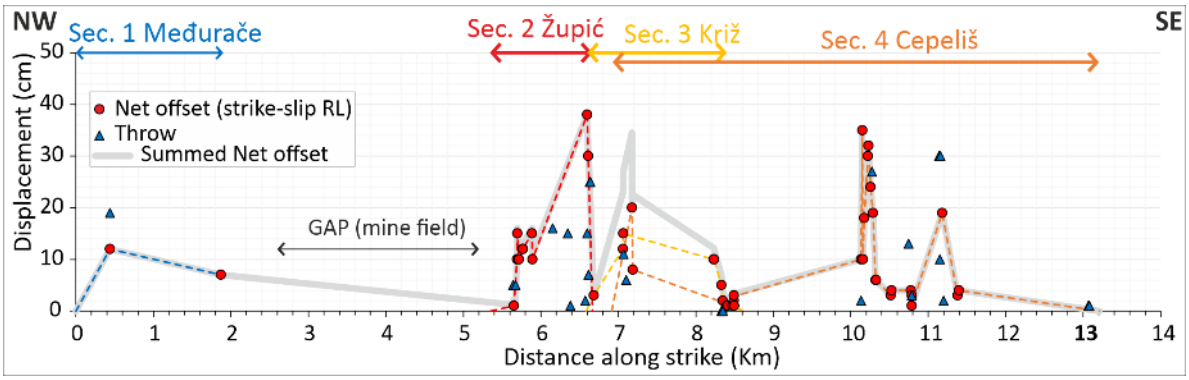

Figure 13. Along-strike slip distribution profile. Red circles and blue triangles are net offset (right-lateral) and throw values, respectively, perpendicularly projected on a 125° striking baseline. Dashed colored lines connect points of net offset of each fault section. The thick grey line is the cumulative net offset, obtained by summing overlapping sections. The observational gap between 2.5 and 5 km is due to an uncleared minefield.

3.2 Liquefaction

The Mw 6.4 earthquake of Petrinja affected a region of lowlands with widespread wet alluvial plains and marshes. Earthquake shaking triggered extensive liquefaction and lateral spreading phenomenon within approximately 20 km around the epicenter, covering an area of ~600 km² (Fig. 6) (Amoroso et al., 2021). In order to provide a detailed identification of the liquefaction features, field reconnaissance campaigns, coupled with analyses of drone survey images and satellite photos, were performed immediately post-event up to March 2021 (Fig. 14). Data from the surveys resulted in the collection of about 200 liquefaction features with the highest possible completeness both in terms of description and distribution of the phenomena (e.g., typology, thickness, extent, type of ejecta etc.). Typology of those features includes (1) blows of sands and/or gravels with the local presence of shells and armored mud balls, (2) lateral spreading phenomenon along road and river embankments, as well as sand ejecta of different grain size and matrix, even at the same site; and (3) sand and/or gravel ejecta along fissures.

The liquefaction distribution, occurring mainly along paleochannel deposits, refers to phenomena related to the fluvial environment of Kupa, Sava and Glina rivers (Figs. 14C and 14D). The liquefaction

features are generally and consistently aligned over large distances, following the trend of the present fluvial system or of abandoned river features. At some places near the riverbanks, we observed fractures with large openings, sometimes accompanied by few centimeters of lateral or vertical displacement and liquefaction ejecta. Locally the liquefaction features are curvilinear along abandoned meanders (see Supplementary Material S3, e.g. areas 1 and 2). The thickness of the extruded ejecta was up to approximately 90 cm, the maximum observed diameter of individual volcanoes was 3 m; and the coalescent sand blows along fractures extended for a maximum length of about 150 m. Ejecta were characterized by different grain size, matrix and color even at the same site, suggesting possible different sources or sand sorting. To address this point, ejecta were sampled at selected sites to perform laboratory tests (i.e. petrographic and geotechnical analyses). We identified our gravel liquefaction sites between the easternmost fault trace (section 4) and the city of Petrinja, also detecting the local presence of shells and armored mud balls (an example is reported in Fig. 14D). Gravel ejecta, typically 20 to 70% gravel according to the 4.75-mm particle size criterion, are rare and were previously detected only following a few seismic events, e.g., in the 1976 Friuli (Italy) earthquake (Rollins et al., 2020). Lateral spreading phenomena were also surveyed along roads and river embankments (Figure 14B).

We analyzed the arrangement of liquefaction features over the whole epicentral area based on drone surveys and Google Earth images available after the earthquakes. We conclude that these are spread over the alluvial plain near the Kupa, Glina and Sava rivers (Fig. 14). Best examples are found north of Sisak, along the Sava River at the locality of Palanjek (Area 3 in Supplementary Material S3), where we captured a drone view of an outstanding set of open and en échelon fissures, either left-stepping or right-stepping, with massive ejecta and tiny left-lateral offsets (1 cm). They are striking 80°, parallel to the Sava River bank. In the northernmost area that was surveyed (Letovanic, Area 4 in Suppl. Mat. S3), the alluvial plain is disrupted by 100-200 m long sets of open (up to 20 cm) and deep (75 cm) fissures, locally associated with sand volcanoes. Ejecta are massive in terms of volume. Some fissures have significant throw (~10 cm) or locally slight right-lateral offset (4 cm). They are striking

parallel to the current Kupa River and to an abandoned meander (N80° to N100°E) nearby. They have severely damaged roads, houses and their backyards. In Stara Drenčina, between Sisak and Petrinja (Area 2, Supplementary Material S1.3), a series of similar left-stepping open fissures with ejecta are mapped sub-parallel to the Kupa River banks in the alluvial deposits, striking from N10° to N150°.

The opening is large, between 20 to 70 cm wide and fissures can be up to 1 m deep. A right-lateral offset of 5 cm was measured by Tondi et al. (2021). Around Petrinja city and Brest Pokupski (Area 1, Suppl. Mat. S1.3), on each side of the Kupa river, the open fissures are dominantly striking from NE to NNE, showing sandy ejecta for most of them. In places, these fissures show small lateral offsets (2 cm), mostly left-lateral with rare cases of right-lateral motion. Locally, we also measured the vertical throw (5 cm) associated with the fractures. On embanked roads, fractures, mostly without ejecta, almost systematically strike perpendicularly to the road axis, suggesting a control by settlement or refraction due to mechanical contrast. Such fractures, often associated with ejecta, are developed by a combination of tensional forces and sometimes a bit of shear. Noticeably, they occur beyond the maximum ground deformation area as inferred from InSAR signal (Section 2.2, Figure 3) and follow the trend of the fluvial channels or abandoned meanders (Fig. 15 and Supplementary Material S3). Due to their arrangements and location, such liquefaction-related features represent hydraulic fractures, occurring due to shaking-related overpressure of confined shallow sandy aquifers. Such overpressure increases the size, extent, and connectivity of existing fractures or breaks apart stratigraphic heterogeneities, as well as triggers gravitational instabilities at embankments (i.e. lateral spreading).

Preliminary considerations reveal that the available empirical relationships between magnitude and epicentral distance or lateral extent of liquefaction (Ambraseys, 1988; Galli, 2000; Maurer et al., 2015) are in good agreement with the features observed after the Petrinja earthquake. However, considering the huge amount of data collected, the liquefaction dataset is still under elaboration and, once completed, it could assist in updating the existing empirical relationships and building new

ones, and mitigate the effects of future earthquakes, as for seismic microzonation studies. Moreover, these liquefaction features appear similar to those from recent earthquakes of similar magnitude (Mw around 6) and shallow (< 10 km) earthquakes without principal surface ruptures, such as the 2012 Emilia (Italy) (Civico et al., 2015), the 2021 Central Thessaly (Greece) (Valkaniotis et al., 2021) or the 2016 Pawnee earthquake (Eastern USA) (Kolawole et al., 2017). These earthquakes induced widespread liquefaction phenomenon in the alluvial plains in an area of about 20 km from the epicenter, resulting in aligned and *en échelon* fractures along paleochannels (e.g. see Amoroso et al., 2020; Civico et al., 2015 for details regarding the 2012 Emilia earthquake).

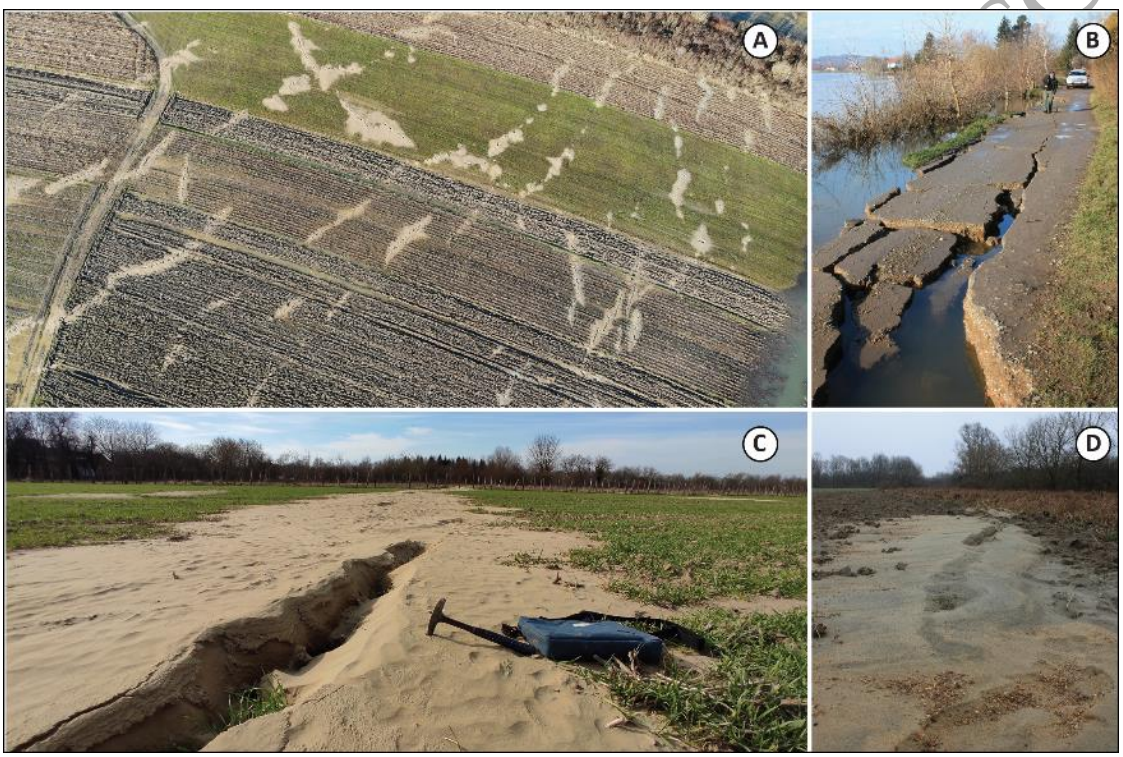

Figure 14: Examples of liquefaction following the Petrinja earthquake: (A) aerial view from drone at Letovanić (area 4 on Figure 15); (B) lateral spreading along Kupa river embankment at Letovanić (area 4 on Figure 15); (C) crack with sand ejecta in the alluvial plain of the Sava river; (d) sand and gravel ejecta of different provenance with presence of shells close to Kupa river.

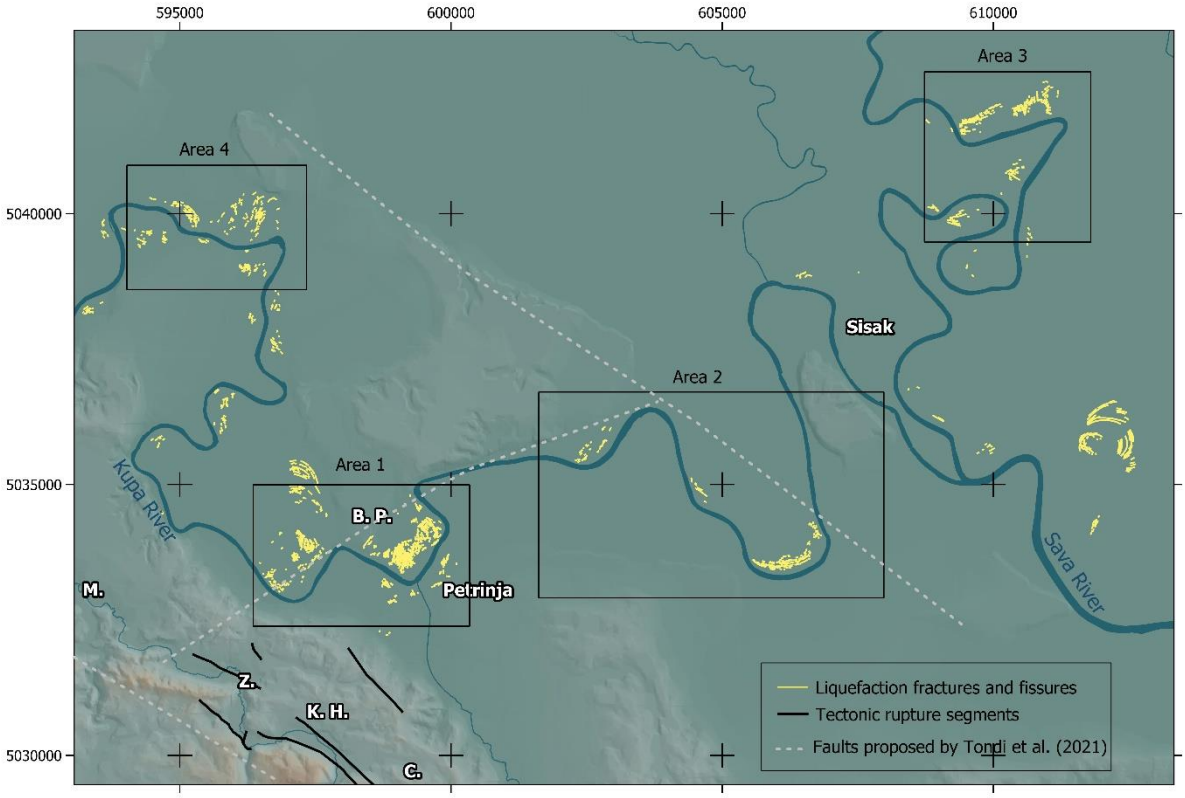

Figure 15. Map of liquefaction-related fissures in the epicentral area (field-checked and remote sensing), around Petrinja and Sisak. Fissures were drawn based on a visual analysis of drone and satellite images (some available on Google Earth). Areas 1 to 4 refers to focused maps and pictures provided in Suppl. Mat. S3. B. P.: Brest Pokupski. Fault lines as inferred by Tondi et al. (2021) are shown in white dashed lines for comparison.

3.3 Slope failures

Slope failures, i.e. landslides and rockfalls, were observed in the field during our survey. Pollak et al. (2021) describe 36 landslides and 4 rockfalls, most of them reactivating pre-existing features. During our field survey, landslides were visible close to the PPKF (Petrinja area, between Cepeliš and Križ Hrastovački, Međurače) and its northern continuation (Stari Farkašić, S. F., on the rim of the Kupa River). Pollack et al. (2021) attribute most of the landslides to the presence of poorly consolidated lithologies included in Pliocene and Plio-Quaternary formations. A large landslide affects the landfill of the big Međurače quarry (Paleogene bedrock) several hundred meters off the surface rupture trace. The landslides that could be checked in the field are of various sizes and amounts of

displacement. We also mapped rockfalls, one of the most important being close to the surface rupture, in Hrastovica, with large boulders of Badenian calcarenites dropped down during earthquake shaking.

Figure 16. Coseismic slope failures caused by the 2020 Petrinja earthquake sequence. Top) The landfill landslide of the Međurače quarry (Paleogene rocks) (ID 434; latitude 45.432899, longitude 16.179700). Bottom) Rockfall located within the fault zone in highly fractured Badenian calcarenites at the head of a gully. West of Hrastovica (ID 170/ latitude 45.3972938, longitude 16.2815195).

Our team contribution to this secondary effect analysis includes also the interpretation of InSAR data (see Section 2.2 for details). The wrapped interferograms, with their fringes, are very helpful in identifying closed areas with small displacement in the Line Of Sight (LOS). Compared to pre-existing morphology (Fig. 17), we suggest those areas could correspond to coseismically reactivated large-scale (~1 km) pre-existing features, such as deep-seated landslides. The two examples show tiny displacements (several cm) which probably would be hard to be identified in the field. During the analysis, we spotted 80 similar cases over a vast area of ~2000 km²; their coordinates are reported in the database (Supplementary Material S1.2).

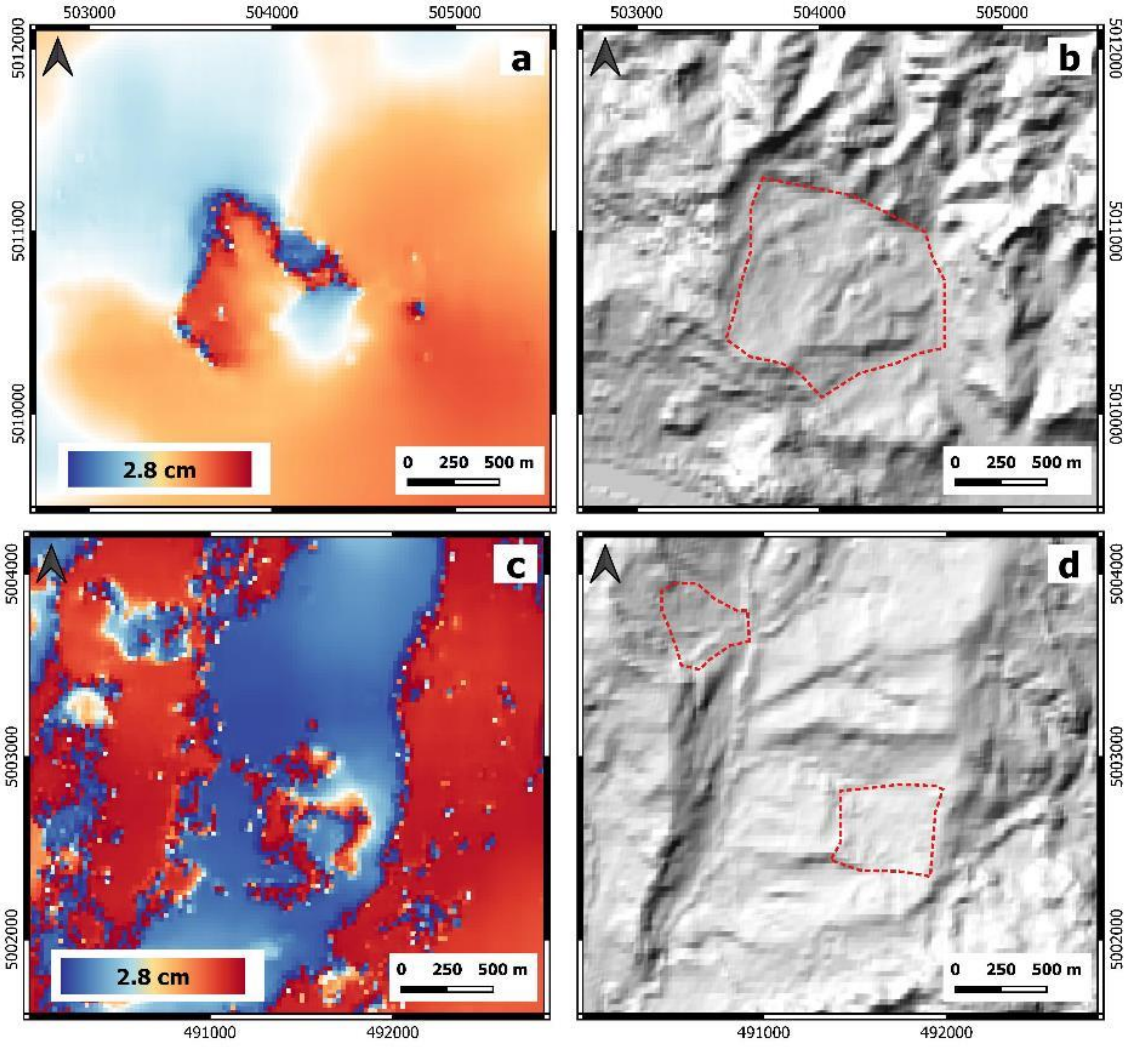

Figure 17. Examples of deep-seated landslides re-activated during the Mw 6.4 earthquake identified using InSAR. Wrapped interferograms (a,c) and the equivalent relief maps (b,d) from Copernicus DEM, with approximate boundaries indicated by red dashed lines. Scale bars show the LOS (Line Of Sight) displacement captured within a full fringe.

4. Discussion

4.1 Surface rupture during the 2020 sequence

We have reconstructed the 2020 earthquake surface rupture in a total length of ~13 km from Međurače to the north to Donja Budičina to the south, a number substantially larger than the one inferred from seismology (Causse, 2021). The surface rupture trace is discontinuous with four main strands, separated by short gaps or left step-overs. The maximum measured dextral offset is 0.38 m, with an average 0.09 to 0.10 m offset, calculating the mean from the integral of the curve or the arithmetic mean, respectively.

A first and preliminary model, based only on remote sensing, suggested the potential absence of surface faulting, with an upper limit of the modelled fault rupture at one kilometer depth, and an 8-km long fault (Ganas et al., 2021). However, our results emphasize that this estimation should be revised. Our analysis also highlights similarly to other recent examples (e.g. Koehler et al., 2021), the importance of field survey and conformation of remote and modelling data after a shallow earthquake. We underline that this is the unique way to compile a robust dataset of surface deformation and to reach a proper level of resolution to describe the rupture complexity. Other studies concluded that a major NE-SW conjugate fault was also involved in the coseismic rupture during the mainshock (see Fig. 15), based on the occurrence of NE-SW striking fissures with tiny lateral offsets (max. 2 cm) at a few sites (Markušić et al., 2021; Tondi et al., 2021), or based on the geodetic signal (Bjelotomić Oršulić et al., 2021). Conversely, our widespread analysis reveals that the fissures invoked by these authors are developed independently from surface traces of active faults, but consistently with fluvial landforms. Actually, our InSAR displacement map does not support a NE-SW-oriented source of (near-)surface displacement, and is consistent with inversion models with a single rupture at depth (Causse, 2021; Ganas et al., 2021; Xiong et al., 2021). In addition, our GPS benchmark vector map resembles at first order to the velocity field that would be obtained with the elastic dislocation on a single NW-SE fault (Okada, 1992, 1985). This agrees with our field validation that do not provide unequivocally evidence of a conjugate fault to the PPKF, because the

deformation indices are not spatially and kinematically coherent with such a NE-SW left-lateral fault. Indeed, they spread around the Sava and Kupa rivers, over a much broader area than presented by those authors, and their spatial distribution aligns or follows ancient and current fluvial bars, meanders, oxbow lake rims, etc. We suggest that the aforementioned NE-SW features are most probably related to liquefaction and/or lateral spreading, where a gentle slope may favor minor lateral displacement along the downslope oriented fractures (e.g. Dobry et al., 2011). Alternatively, it may be possible that these fissures represent local adjustments to in-volume coseismic strain and be grouped into short and distributed ruptures. Altogether, we do not endorse the existence of any NE-SW "cross" or "conjugate" left-lateral fault(s) between Petrinja and Sisak, as suggested by previous authors (Bjelotomić Oršulić et al., 2021; Markušić et al., 2021; Tondi et al., 2021). In addition, the parallel right-lateral fault to the east, proposed by Tondi et al. (2021) as a leading tectonic feature during coseismic strain accommodation, has no support from surface geodetic data and field observations. Actually, the geological features (fissures, liquefaction features) are small scale ones, without any continuation to the NW and SE. The occurrence of an aftershock cluster off the principal rupture between Petrinja and Sisak (contour shown on Fig. 3), (Stipčević et al., 2021), does not seem to be a potential source for surficial surface deformation either, considering the timing (most of the events occurred after the surface deformation), the cluster depth (from 6 to 29 km) and magnitude values (Ml from 0.9 to 3.5).

Slip measurements were determined at several sites thanks to piercing points or lines. The maximum offsets, dominantly right-lateral, reach the maximum values of 30 cm (strike slip component) and 38 cm (net offset) at the southern tip of the Župić strand, and 20 cm and 15 cm on the two parallel strands around Križ Hrastovački. Similar net offset values are observed on the Cepeliš strand to the south, however with a significant vertical component of probably gravitational origin. Typical offset values are around 10 cm along each segment. Altogether, those data perfectly fit the mean values obtained for an Mw 6.4 earthquake following the empirical relationships of Wells and Coppersmith (1994) for strike-slip earthquakes. We could not find evidence of afterslip in the field but we cannot

exclude that part of the total slip measured could be due to this post-seismic deformation: our InSAR analysis suggests that post-seismic offset, which does not exceed 5-10 cm, could have been a significant part of the total offset along the northernmost section (Međurače), up to the northernmost investigated areas where small right-lateral offsets have been observed close to the Kupa river bank (Stari Farkašić, ID 417).

4.2 Long-term activity of the Petrinja-Pokupsko Fault (PPKF)

During the post-seismic survey, we documented potential evidence for the long-term activity of the PPKF. Geomorphic analysis based on field observations, topographic maps (1:5,000), high resolution post-earthquake LiDAR, Pléiades- and WorldView-derived DEMs (~1 m resolution), seismic-reflection and well data, in combination with available geological data (Pikija, 1987; Šikić, 2014) suggest that the Hrastovica Mountain (see Fig. 3 for location) coincides with a ~5-kilometer-wide zone of uplifted Neogene deposits (~1000 m for Lower Miocene) resulting from dextral-transpressive faulting along the PPKF (see Fig. 2 for illustration). This deformation is expressed in the landscape by the shaping of the drainage network that cross the structure (Henriquet et al., 2021; Jamšek Rupnik et al., 2021), i.e. the incision and aggradation behaviour of streams and the valley shapes, as well as in the seismic profiles where Neogene-Quaternary layers are folded (Fig. 2). Changes of hydrographic network are especially clear for major rivers. In particular, the Petrinjčica, Utinja and their tributary valleys' widths (see Fig. 7a for location), heights, and directions appear to be modified when crossing the fault system. The valleys are broad and shallow in the south-western part, before crossing the uplifted zone where they become deeply incised and narrower, then again the aggradation prevails once leaving the Hrastovica Mountain (see Fig. 7a for location) towards the Kupa lowland in the east. The valleys and the streams also show clear deflection at the transition from the Hrastovica Mountain to the lowland area, where the fault reactivated during the 2020 earthquake sequence emerges to the surface. A detailed tectonic-geomorphologic mapping of fault traces in a short distance to the coseismic surface ruptures reveals right-lateral offsets of drainage features and crests, mostly localized on the southern section of the fault system, south of Župić, with cumulative displacements

ranging from 5 m to more than 500 m. We present here an example of the potential cumulative record at Cepeliš (Fig. 18) within the central sector of the 2020 surface rupture, where fluvial features are incised in Miocene (SW of the fault) to Pliocene (NE of the fault) formations and where we identified two major NW-SE fault segments. Piercing-lines based on stream axis and risers allow a retro-deformation of 260±25 m on the southern branch (P1 and P2, Fig. 18), and possibly up to 290-315 m on the northern branch (P1). As the two branches separated by 200 m likely merge at depth, a total right-lateral displacement of about 560 m is inferred on the PPKF at this location. According to the European database (Basili et al., 2013), the estimated slip rate from geological and geodynamics inferences ranges from 0.08 mm/yr to 0.2 mm/yr. Extrapolating this rate to accommodate the ~560 m cumulative displacement yields an age of 7 to 2.8 Ma, which is compatible with the tectonic inversion of the Pannonian basin initiated in the Upper Miocene to Pliocene (Horváth et al., 2006; Matoš et al., 2014; Tomljenović and Csontos, 2001; Ustaszewski et al., 2010). However, recent studies in the Eastern Alps suggest that the kinematic change of the Adriatic promontory relative to Europe might have occurred later, during the Quaternary, 1–2 Ma ago (Moulin and Benedetti, 2018). Following this, the inferred long-term slip rate along the PPKF could be hypothesized as high as 0.3 mm/yr to 0.6 mm/yr. Further work is needed in the PPKF area to constrain the age of the displaced geomorphic markers and establish robust slip rate estimations.

In addition and preparation for further investigations, the fault segments with evidence of long-term displacement can be compared to the 2020 surface ruptures (Figure 7A), to help in identifying key sites for further paleoseismological investigations. These preliminary results are particularly promising as most of the evidence of surface ruptures are consistent with the mapped fault system. We also note that evidence of coseismic surface rupture north of Župić is rare (except section 1, Figure 7A), precisely where evidences of cumulative right-lateral offsets are sparse while geomorphic features such as perched valleys and wind gaps rather suggest ongoing uplift (Henriquet et al., 2021).

4.3 Seismic hazard(s)

The pattern of deformation, its spatial arrangement and temporal sequence, through tectonic morphology analysis, paleoseismological investigation and dating deposits or surfaces, need to be further explored in detail on the PPKF, as well as their relationships with the 2020 surface rupture segments. This is a necessary step to investigate the long-term fault kinematics, the potential fault system segmentation and the associated slip rate, which are key components of the associated seismic hazard assessment, both in terms of expected ground motion and fault displacement.

The recent 29 December 2020 earthquake confirms the seismic potential of the Petrinja composite source defined by Basili et al. (2013), and its capacity to produce Mw >6 earthquakes. Our study however suggests that this source is essentially a steep fault running along the Hrastovica Mountains, and that the former east-dipping normal faults responsible for the Pannonian basin subsidence are buried beneath the Sava-Kupa alluvial plain. It is also noteworthy that the 2020 Petrinja earthquake sequence occurred only 9 months after the Zagreb March 2020 (Mw 5.3) earthquake on an ENE-WSW-trending thrust fault, broadly orthogonal to the right-lateral Pokupsko fault, ~45 km to the north. A potential interplay between strike-slip and thrust faults in this moderate strain-rate intraplate settings is another target of exploration (Ganas et al., 2021).

The 2020 surface rupture delineate a 13 km long structure, a part of a larger-scale system of NW-SE faults separated by gaps and step-overs (Fig. 1). These individual faults, typically 10-15 km long, delineate a >100 km long system, grouped into the Petrinja-Pokupsko and Prijedor faults in Figure 1. These observations raise many questions, among them whether the faults of the system that did not rupture in 2020 could only be considered as independent seismic sources. Or could the system generate larger earthquakes than the 2020 Petrinja event, mobilizing several faults altogether, like shown historically in other strike-slip environments (e.g. M7.5 Landers earthquake in 1992)? In any case, future seismic hazard models should include geologically-derived slip rates for this apparently segmented fault system, supported by extensive paleoseismological investigations.

Finally, the coseismic effect dataset of the Petrinja earthquake will contribute to the international and unified database effort that aggregates worldwide historical and recent events (Baize et al., 2020; Nurminen et al., 2020; Sarmiento et al., 2021).

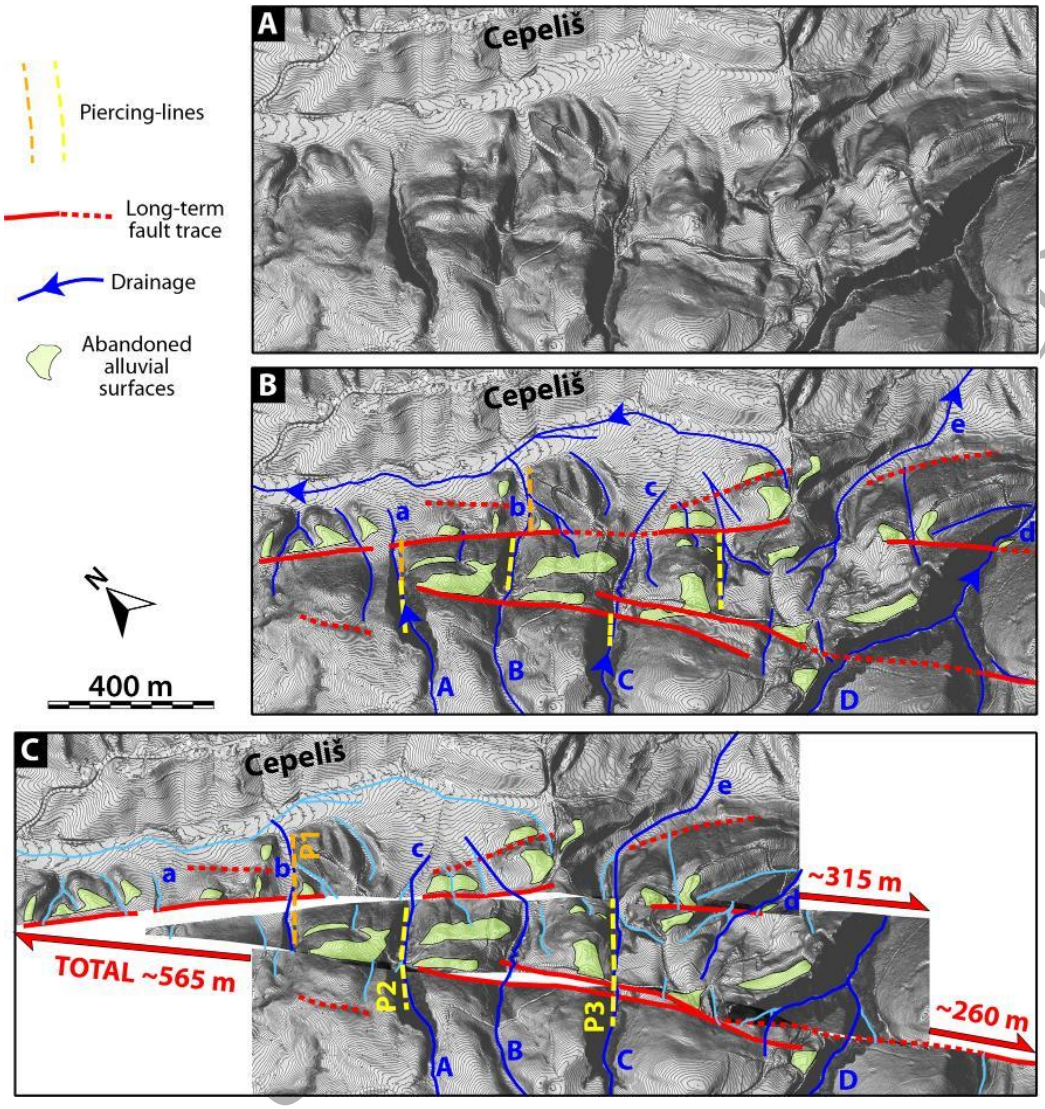

Figure 18: Shaded 1 m LiDAR DEM with 1 m contour lines (A), geomorphological imprint of the long-term fault segments at Cepeliš (B) and possible retro-deformation model (C). Fault segments are shown in red. The drainage network (blue) and low angle slopes interpreted as abandoned alluvial surfaces (light green) are also represented. Piercing-lines for measuring river axis and riser offsets are shown in orange (P1) and yellow (P2 and P3) for the northern and southern fault branches, respectively. 260±25 m of retro-deformation is constrained on the southern branch using P2 and P3 piercing-lines, and a maximum back-slipping of 290-315 m is estimated on the northern branch from the P1 piercing-line. Downstream (lowercase letters) and upstream (uppercase letters) segments help to reconstruct a possible paleo-drainage network.

Conclusion

The assembling of a European team, bringing together regional field geologists and specialists in the geological effects of earthquakes, was a key element of this study in order to produce an accurate and complete mapping of the earthquake environmental effects. This collaborative strategy is to be preferred when strong earthquakes occur, in hard-to-reach regions which require a large and rapid mobilization of field earth scientists. Historically, successful examples of a large team surveying earthquake effects were those of 1983 Borah Peak (Crone et al., 1987), 1992 Landers (Hart et al., 1993) earthquakes for instance, all located in the western United States. More recently, large survey teams were deployed during the 2016 Central Italy sequence, the 2016 Kaikoura earthquake and the 2019 Ridgecrest doublet, which have made it possible to collect a great wealth of information. Our initiative is similar. The European continent is still without a federated and formalized group, and the 2016 Italian and this 2020-21 Croatian experiences are exceptions. We claim that it is important to establish a sustainable network of scientists, in order to carry out this kind of investigation in the future, in case of a large event.

Indeed, this type of research locates, describes, quantifies the deformation on the surface, is crucial to understand and characterize the source of major surface-rupturing earthquakes or even blind earthquakes (as for liquefaction evidence), in addition to seismological and geodetic data. It also provides data to constrain the scaling relationships used in paleoseismological studies. These relationships are needed to link geological observations of ancient deformations to the source earthquakes that generated them. Details of surface breaks are also used to develop empirical fault displacement prediction relationships, useful for planning infrastructures (dams, pipelines, installations) that are located near active faults.

The observations made, mainly in the field, at Petrinja make it possible to confirm unambiguously that the deformations measured on the surface, despite their discontinuity and apparent complexity, are related to the seismic rupture in depth, in terms of kinematics (right-lateral fault) and geometry

(segmented rupture). They show that the rupture occurred on an active fault, the Petrinja-Pokupsko Fault (PPKF), which is identified in the morphology. The next steps will be to explore the history of this fault and, where possible, investigate additional structures that extend it north and south. In particular, the slip rate has to be estimated using further observations, such as those of offset and datable geological surfaces. Quantifying the slip rate is particularly important for future seismic hazard models because it constrains the rate of earthquake production. Similarly, for example, it will be possible to estimate the ages of the surface-rupturing paleoearthquakes on different fault segments, and thus consider scenarios of multi-segment earthquakes.

Acknowledgements

The authors are very grateful to the two reviewers (Paula Cristina Figueiredo and Christoph Grützner) who have, thanks to their remarks, comments and corrections, significantly improved this manuscript.

Funding of field survey campaigns was supported by the involved institutes (IRSN, CNRS, University of Chieti-Pescara, INGV, HGI), which covered the expenses of their own personnel. Most of the GeoZS personnel involved was financed by the Slovenian Research Agency, programs P1—0011 and P1-0419.

LiDAR data was acquired after the earthquake with funding from CNRS, University of Chieti, HGI and GeoZS.

The research could not be done without the donation of the academic license of the Petrel E&P software platform from Schlumberger, and data usage permission assigned by the Croatian Hydrocarbon Agency. Most of the maps were designed with QGIS, and the 3D representation was made with Move. David Rukavina helps us interpret syn-rift structures in means of consultation. He is an expert in syn-rift tectonics.

The author contribution is as following: SB ensured the animation of the group; SB, SA, NB, LB, PB, MB, FRC, MH, PJR, BK, SM, LM, DP, SP, MŠ, AT, SV, MV participated to the data collection, in the field or remotely, analyzed those data, participated to the online meetings for the paper preparation and to the writing of the database, and SB, SP, AT worked on the quality insurance of the database. The second part of the list of co-authors (JA, JB, MB, RB, VB, MC, BC, RC, PMDM, RF, FI, AM, MM, TK, RN, AN, MN, BP, DP, TR) were actively working in the field to the data collection or to the remote collection of them. All authors reviewed the manuscript.

Data availability

SAR images were freely downloaded from the European Spatial Agency site (Copernicus). Seismological data were provided by the Department of Geophysics (Faculty of Science, University of Zagreb). The data collected in the field are available on the Zenodo repository: https://doi.org/10.5281/zenodo.5089914. Seismic lines are stored and can be freely requested to the Croatian Hydrocarbon Agency CHA (https://www.azu.hr/en) for scientific purposes.

Reference list

Ambraseys, Jackson, 1998. Faulting associated with historical and recent earthquakes in the Eastern Mediterranean region. Geophys. J. Int. 133, 390–406. https://doi.org/10.1046/j.1365-246X.1998.00508.x

Ambraseys, N.N., 1988. Engineering seismology: Part II. Earthquake Engng. Struct. Dyn. 17, 51–105. https://doi.org/10.1002/eqe.4290170102

Amoroso, S., Barbača, J., Belić, N., Kordić, B., Brčić, V., Budić, M., Civico, R., De Martini, P.M., Hećej, N., Kurečić, T., Minarelli, L., Novosel, T., Palenik, D., Pantosti, D., Pucci, S., Filjak, R., Ricci, T., Špelić, M., Vukovski, M., 2021. Liquefaction field reconnaissance following the 29th December 2020 Mw 6.4 Petrinja earthquake (Croatia) (other). pico. https://doi.org/10.5194/egusphere-egu21-16584

Amoroso, S., Rollins, K.M., Andersen, P., Gottardi, G., Tonni, L., García Martínez, M.F., Wissmann, K., Minarelli, L., Comina, C., Fontana, D., De Martini, P.M., Monaco, P., Pesci, A., Sapia, V., Vassallo, M., Anzidei, M., Carpena, A., Cinti, F., Civico, R., Coco, I., Conforti, D., Doumaz, F., Giannattasio, F., Di Giulio, G., Foti, S., Loddo, F., Lugli, S., Manuel, M.R., Marchetti, D., Mariotti, M., Materni, V., Metcalfe, B., Milana, G., Pantosti, D., Pesce, A., Salocchi, A.C., Smedile, A., Stefani, M., Tarabusi, G., Teza, G., 2020. Blast-induced liquefaction in silty sands for full-scale testing of ground improvement methods: Insights from a multidisciplinary study. Engineering Geology 265, 105437. https://doi.org/10.1016/j.enggeo.2019.105437

Atanackov, J., Jamšek Rupnik, P., Jež, J., Celarc, B., Novak, M., Milanič, B., Markelj, A., Bavec, M., Kastelic, V., 2021. Database of Active Faults in Slovenia: Compiling a New Active Fault Database at the Junction Between the Alps, the Dinarides and the Pannonian Basin Tectonic Domains. Front. Earth Sci. 9, 604388. https://doi.org/10.3389/feart.2021.604388

Baize, S., Nurminen, F., Sarmiento, A., Dawson, T., Takao, M., Scotti, O., Azuma, T., Boncio, P., Champenois, J., Cinti, F.R., Civico, R., Costa, C., Guerrieri, L., Marti, E., McCalpin, J., Okumura, K., Villamor, P., 2020. A Worldwide and Unified Database of Surface Ruptures (SURE) for Fault Displacement Hazard Analyses. Seismological Research Letters 91, 499–520. https://doi.org/10.1785/0220190144

Basili, R., Kastelic, V., Demircioglu, M.B., Garcia Moreno, D., Nemser, E.S., Petricca, P., Sboras, S.P., Besana-Ostman, G.M., Cabral, J., Camelbeeck, T., Caputo, R., Danciu, L., Domaç, H., Fonseca, J.F. de B.D., García-Mayordomo, J., Giardini, D., Glavatovic, B., Gulen, L., Ince, Y., Pavlides, S., Sesetyan, K., Tarabusi, G., Tiberti, M.M., Utkucu, M., Valensise, G., Vanneste, K., Vilanova, S.P., Wössner, J., 2013. European Database of Seismogenic Faults (EDSF). https://doi.org/10.6092/INGV.IT-SHARE-EDSF

Bjelotomić Oršulić, O., Markovinović, D., Varga, M., Bašić, T., 2021. Coseismic Ground Displacement after the Mw 6.2 Earthquake in NW Croatia Determined from Sentinel-1 and GNSS CORS Data. Geosciences 11, 170. https://doi.org/10.3390/geosciences11040170

Causse, M., 2021. Rupture analysis of the 2020 Petrinja earthquake based on seismological observations (other). pico. https://doi.org/10.5194/egusphere-egu21-16577

Civico, R., Brunori, C.A., De Martini, P.M., Pucci, S., Cinti, F.R., Pantosti, D., 2015. Liquefaction susceptibility assessment in fluvial plains using airborne lidar: the case of the 2012 Emilia earthquake sequence area (Italy). Nat. Hazards Earth Syst. Sci. 15, 2473–2483. https://doi.org/10.5194/nhess-15-2473-2015

Civico, R., Pucci, S., Villani, F., Pizzimenti, L., De Martini, P.M., Nappi, R., the Open EMERGEO Working Group, 2018. Surface ruptures following the 30 October 2016 Mw 6.5 Norcia earthquake, central Italy. Journal of Maps 14, 151–160. https://doi.org/10.1080/17445647.2018.1441756

Crone, A.J., Machette, M.N., Bonilla, M.G., Lienkaemper, J.J., Pierce, K.L., Scott, W.E., Bucknam, R.C., 1987. Surface faulting accompanying the Borah Peak earthquake and segmentation of the lost river fault, central Idaho. Bulletin of the Seismological Society of America 77, 739–770.

Dobry, R., Thevanayagam, S., Medina, C., Bethapudi, R., Elgamal, A., Bennett, V., Abdoun, T., Zeghal, M., El Shamy, U., Mercado, V.M., 2011. Mechanics of Lateral Spreading Observed in a Full-Scale Shake Test. J. Geotech. Geoenviron. Eng. 137, 115–129. https://doi.org/10.1061/(ASCE)GT.1943-5606.0000409

DuRoss, C.B., Gold, R.D., Dawson, T.E., Scharer, K.M., Kendrick, K.J., Akciz, S.O., Angster, S.J., Bachhuber, J., Bacon, S., Bennett, S.E.K., Blair, L., Brooks, B.A., Bullard, T., Burgess, W.P., Chupik, C., DeFrisco, M., Delano, J., Dolan, J.F., Frost, E., Graehl, N., Haddon, E.K., Hatem, A.E., Hernandez, J.L., Hitchcock, C., Hudnut, K., Thompson Jobe, J., Koehler, R., Kozaci, O., Ladinsky, T., Madugo, C., McPhillips, D.S., Milliner, C., Morelan, A., Olson, B., Patton, J., Philibosian, B., Pickering, A.J., Pierce, I., Ponti, D.J., Seitz, G., Spangler, E., Swanson, B., Thomas, K., Treiman, J., Valencia, F., Williams, A., Zinke, R., 2020. Surface Displacement Distributions for the July 2019 Ridgecrest, California, Earthquake Ruptures. Bulletin of the Seismological Society of America 110, 1400–1418. https://doi.org/10.1785/0120200058

Galli, P., 2000. New empirical relationships between magnitude and distance for liquefaction. Tectonophysics 324, 169–187. https://doi.org/10.1016/S0040-1951(00)00118-9

Ganas, A., Elias, P., Valkaniotis, S., Tsironi, V., Karasante, I., Briole, P., 2021. Petrinja earthquake moved crust 10 feet. Temblor. https://doi.org/10.32858/temblor.156

Grünthal, G., Wahlström, R., Stromeyer, D., 2013. The SHARE European Earthquake Catalogue (SHEEC) for the time period 1900–2006 and its comparison to the European-Mediterranean Earthquake Catalogue (EMEC). J Seismol 17, 1339–1344. https://doi.org/10.1007/s10950-013-9379-y

Hart, E.W., Bryant, W.A., Treiman, J.A., 1993. Surface faulting associated with the June 1992 Landers earthquake, California. California Geology 46, 10–16.
Henriquet, M., Moulin, A., Vukovski, M., Kordić, B., Budić, M., Hollingsworth, J., Gold, R., Baize, S., Benedetti, L., 2021. Comparison between the coseismic surface displacement during the 29 December 2020 Mw 6.4 Petrinja earthquake (Croatia) from optical image correlation and long-term geomorphological observations of cumulative displacements (other). pico. https://doi.org/10.5194/egusphere-egu21-16590
Herak, D., Herak, M., 2010. The Kupa Valley (Croatia) Earthquake of 8 October 1909--100 Years Later. Seismological Research Letters 81, 30–36. https://doi.org/10.1785/gssrl.81.1.30
Herak, D., Herak, M., Tomljenović, B., 2009. Seismicity and earthquake focal mechanisms in North-Western Croatia. Tectonophysics 465, 212–220. https://doi.org/10.1016/j.tecto.2008.12.005
Herak, M., Herak, D., Markušić, S., 1996. Revision of the earthquake catalogue and seismicity of Croatia, 1908?1992. Terra Nova 8, 86–94. https://doi.org/10.1111/j.1365-3121.1996.tb00728.x
Horváth, F., Bada, G., Szafián, P., Tari, G., Ádám, A., Cloetingh, S., 2006. Formation and deformation of the Pannonian Basin: constraints from observational data. Geological Society, London, Memoirs 32, 191–206. https://doi.org/10.1144/GSL.MEM.2006.032.01.11
Jamšek Rupnik, P., Budić, M., Vukovski, M., Kordić, B., Špelić, M., Belić, N., Palenik, D., Bočić, N., Atanackov, J., Celarc, B., Novak, A., Novak, M., Brajkovič, R., Bavec, M., Baize, S., 2021. Some geomorphological perspectives on the structure associated with the Petrinja M6.2 earthquake in Croatia (other). pico. https://doi.org/10.5194/egusphere-egu21-16578
Koehler, R.D., Dee, S., Elliott, A., Hatem, A., Pickering, A., Pierce, I., Seitz, G., 2021. Field Response and Surface-Rupture Characteristics of the 2020 M 6.5 Monte Cristo Range Earthquake, Central Walker Lane, Nevada. Seismological Research Letters 92, 823–839. https://doi.org/10.1785/0220200371
Kolawole, F., Atekwana, E.A., Ismail, A., 2017. Near-Surface Electrical Resistivity Investigation of Coseismic Liquefaction-Induced Ground Deformation Associated with the 2016 M_w 5.8 Pawnee, Oklahoma, Earthquake. Seismological Research Letters 88, 1017–1023. https://doi.org/10.1785/0220170004
Kordić, B., Lužar-Oberiter, B., Pikelj, K., Matoš, B., Vlastelica, G., 2019. Integration of Terrestrial Laser Scanning and UAS Photogrammetry in Geological Studies: Examples from Croatia. Period. Polytech. Civil Eng. https://doi.org/10.3311/PPci.14499
Kreemer, C., Blewitt, G., Klein, E.C., 2014. A geodetic plate motion and Global Strain Rate Model. Geochemistry, Geophysics, Geosystems 15, 3849–3889. https://doi.org/10.1002/2014GC005407
Markušić, S., Stanko, D., Korbar, T., Belić, N., Penava, D., Kordić, B., 2020. The Zagreb (Croatia) M5.5 Earthquake on 22 March 2020. Geosciences 10, 252. https://doi.org/10.3390/geosciences10070252
Markušić, S., Stanko, D., Penava, D., Ivančić, I., Bjelotomić Oršulić, O., Korbar, T., Sarhosis, V., 2021. Destructive M6.2 Petrinja Earthquake (Croatia) in 2020—Preliminary Multidisciplinary Research. Remote Sensing 13, 1095. https://doi.org/10.3390/rs13061095
Matoš, B., Tomljenović, B., Trenc, N., 2014. Identification of tectonically active areas using DEM: a quantitative morphometric analysis of Mt. Medvednica, NW Croatia. GQ 58. https://doi.org/10.7306/gq.1130
Maurer, B.W., Green, R.A., Cubrinovski, M., Bradley, B.A., 2015. Assessment of CPT-based methods for liquefaction evaluation in a liquefaction potential index framework. Géotechnique 65, 328–336. https://doi.org/10.1680/geot.SIP.15.P.007
McCalpin, J. (Ed.), 2009. Paleoseismology, 2nd ed. ed, International geophysics series. Academic Press, Burlington, MA.
Métois, M., D'Agostino, N., Avallone, A., Chamot-Rooke, N., Rabaute, A., Duni, L., Kuka, N., Koci, R., Georgiev, I., 2015. Insights on continental collisional processes from GPS data: Dynamics of

the peri-Adriatic belts. J. Geophys. Res. Solid Earth 120, 8701–8719. https://doi.org/10.1002/2015JB012023
Michetti, A.M., Esposito, E., Guerrieri, L., Profido, S., Serva, L., Tatevossian, R., Vittori, E., Audemard, F., Azuma, T., Clague, J., Comerci, V., Gürpinar, A., McCalpin, J., Mohammadioun, B., Mörner, N.A., Ota, Y., Roghozin, E., 2007. Environmental Seismic Intensity scale— ESI 2007. Mem. Descr. Carta Geol. D'Ital. 74, 7–23.
Mohorovičić, A., 1992. Potres od 8. X. 1909 (Earthquake of 8 October 1909). Geofizika 9, 3–53.
Moss, R.E.S., Buelna, M., Stanton, K.V., 2018. Physical, Analytical, and Numerical Modeling of Reverse-Fault Displacement through Near-Surface SoilsPhysical, Analytical, and Numerical Modeling of Reverse-Fault Displacement through Near-Surface Soils. Bulletin of the Seismological Society of America 108, 3149–3159. https://doi.org/10.1785/0120180067
Moulin, A., Benedetti, L., 2018. Fragmentation of the Adriatic Promontory: New Chronological Constraints From Neogene Shortening Rates Across the Southern Alps (NE Italy). Tectonics 37, 3328–3348. https://doi.org/10.1029/2018TC004958
Moulin, A., Benedetti, L., Rizza, M., Jamšek Rupnik, P., Gosar, A., Bourlès, D., Keddadouche, K., Aumaître, G., Arnold, M., Guillou, V., Ritz, J.-F., 2016. The Dinaric fault system: Large-scale structure, rates of slip, and Plio-Pleistocene evolution of the transpressive northeastern boundary of the Adria microplate: THE DINARIC FAULTS SYSTEM (NE ADRIA). Tectonics 35, 2258–2292. https://doi.org/10.1002/2016TC004188
Nocquet, J.-M., 2012. Present-day kinematics of the Mediterranean: A comprehensive overview of GPS results. Tectonophysics 579, 220–242. https://doi.org/10.1016/j.tecto.2012.03.037
Nurminen, F., Boncio, P., Visini, F., Pace, B., Valentini, A., Baize, S., Scotti, O., 2020. Probability of Occurrence and Displacement Regression of Distributed Surface Rupturing for Reverse Earthquakes. Front. Earth Sci. 8, 581605. https://doi.org/10.3389/feart.2020.581605
Obermeier, S.F., 1996. Chapter 7 Using liquefaction-induced features for paleoseismic analysis, in: International Geophysics. Elsevier, pp. 331–396. https://doi.org/10.1016/S0074-6142(96)80074-X
Okada, Y., 1992. Internal deformation due to shear and tensile faults in a half-space. Bulletin of the Seismological Society of America 82, 1018–1040.
Okada, Y., 1985. Surface deformation due to shear and tensile faults in a half-space. Bulletin of the Seismological Society of America 75, 1135–1154.
Pavasović, M., Marjanović, M., Bašić, T., 2016. Towards the new Croatian terrestrial reference frame based on CROPOS - preliminary results. Teh. vjesn. 23. https://doi.org/10.17559/TV-20141114153027
Pavičić, I., Rukavina, D., Matoš, B., Tomljenović, B., 2019. Interpretation of the tectonic evolution of the western part of the Sava Depression: structural analysis of seismic attributes and subsurface structural modeling. Journal of Maps 15, 733–743. https://doi.org/10.1080/17445647.2019.1663374
Pikija, M., 1987. Basic Geological Map of SFRY 1:100.000, Sisak sheet. Geol. Zavod, Zagreb, Savezni geol. Zavod, Beograd.
Placer, L., Vrabec, M., Celarc, B., 2010. The bases for understanding of the NW Dinarides and Istria Peninsula tectonics. Geologija 53, 55–86. https://doi.org/10.5474/geologija.2010.005
Pollak, D., Gulam, V., Novosel, T., Avanić, R., Tomljenović, B., Hećej, N., Terzić, J., Stipčević, J., Bačić, M., Kurečić, T., Dolić, M., Bostjančić, I., Wacha, L., Kosović, I., Budić, M., Vukovski, M., Belić, N., Špelić, M., Brčić, V., Barbača, J., Kordić, B., Palenik, D., Filjak, R., Frangen, T., Pavić, M., Urumović, K., Sečanj, M., Matoš, B., Govorčin, M., Kovačević, M.S., Librić, L., 2021. The preliminary inventory of coseismic ground failures related to December 2020 – January 2021 Petrinja earthquake series. Geol Cro 74. https://doi.org/10.4154/gc.2021.08
Pousse-Beltran, L., Nissen, E., Bergman, E.A., Cambaz, M.D., Gaudreau, É., Karasözen, E., Tan, F., 2020. The 2020 Mw 6.8 Elazığ (Turkey) Earthquake Reveals Rupture Behavior of the East Anatolian Fault. Geophys. Res. Lett. 47. https://doi.org/10.1029/2020GL088136

Quigley, M.C., Hughes, M.W., Bradley, B.A., van Ballegooy, S., Reid, C., Morgenroth, J., Horton, T., Duffy, B., Pettinga, J.R., 2016. The 2010–2011 Canterbury Earthquake Sequence: Environmental effects, seismic triggering thresholds and geologic legacy. Tectonophysics 672–673, 228–274. https://doi.org/10.1016/j.tecto.2016.01.044

Rollins, K.M., Amoroso, S., Milana, G., Minarelli, L., Vassallo, M., Di Giulio, G., 2020. Gravel Liquefaction Assessment Using the Dynamic Cone Penetration Test Based on Field Performance from the 1976 Friuli Earthquake. J. Geotech. Geoenviron. Eng. 146, 04020038. https://doi.org/10.1061/(ASCE)GT.1943-5606.0002252

Sarmiento, A., Baize, S., Boncio, P., Bozorgnia, Y., Dawson, T., Lavrentiadis, G., Madugo, C., Nurminen, F., Shen, A., Thompson, S., 2021. A Next-Generation Fault Displacement and Surface Rupture Database. Presented at the Seismological Society of America 2021 Annual Meeting. https://doi.org/10.1785/0220210025

Schmid, S.M., Fügenschuh, B., Kounov, A., Maţenco, L., Nievergelt, P., Oberhänsli, R., Pleuger, J., Schefer, S., Schuster, R., Tomljenović, B., Ustaszewski, K., van Hinsbergen, D.J.J., 2020. Tectonic units of the Alpine collision zone between Eastern Alps and western Turkey. Gondwana Research 78, 308–374. https://doi.org/10.1016/j.gr.2019.07.005

Serpelloni, E., Vannucci, G., Anderlini, L., Bennett, R.A., 2016. Kinematics, seismotectonics and seismic potential of the eastern sector of the European Alps from GPS and seismic deformation data. Tectonophysics 688, 157–181. https://doi.org/10.1016/j.tecto.2016.09.026

Šikić, K., 2014. Basic Geological Map of Republic Croatia 1:100.000, Geology of the Bosanski Novi sheet. Croatian Geological Survey.

Stipčević, J., Poggi, V., Herak, M., Parolai, S., Herak, D., Dasović, I., Bertoni, M., Barnaba, C., Pesaresi, D., 2021. First results from temporary deployment of small seismic network following the Mw =6.4 Petrinja earthquake (other). pico. https://doi.org/10.5194/egusphere-egu21-16579

Stucchi, M., Rovida, A., Gomez Capera, A.A., Alexandre, P., Camelbeeck, T., Demircioglu, M.B., Gasperini, P., Kouskouna, V., Musson, R.M.W., Radulian, M., Sesetyan, K., Vilanova, S., Baumont, D., Bungum, H., Fäh, D., Lenhardt, W., Makropoulos, K., Martinez Solares, J.M., Scotti, O., Živčić, M., Albini, P., Batllo, J., Papaioannou, C., Tatevossian, R., Locati, M., Meletti, C., Viganò, D., Giardini, D., 2013. The SHARE European Earthquake Catalogue (SHEEC) 1000–1899. J Seismol 17, 523–544. https://doi.org/10.1007/s10950-012-9335-2

Tomljenović, B., Csontos, L., 2001. Neogene–Quaternary structures in the border zone between Alps, Dinarides and Pannonian Basin (Hrvatsko zagorje and Karlovac Basins, Croatia). Int J Earth Sci 90, 560–578. https://doi.org/10.1007/s005310000176

Tondi, E., Blumetti, A.M., Čičak, M., Di Manna, P., Galli, P., Invernizzi, C., Mazzoli, S., Piccardi, L., Valentini, G., Vittori, E., Volatili, T., 2021. 'Conjugate' coseismic surface faulting related with the 29 December 2020, Mw 6.4, Petrinja earthquake (Sisak-Moslavina, Croatia). Sci Rep 11, 9150. https://doi.org/10.1038/s41598-021-88378-2

Ustaszewski, K., Herak, M., Tomljenović, B., Herak, D., Matej, S., 2014. Neotectonics of the Dinarides–Pannonian Basin transition and possible earthquake sources in the Banja Luka epicentral area. Journal of Geodynamics 82, 52–68. https://doi.org/10.1016/j.jog.2014.04.006

Ustaszewski, K., Kounov, A., Schmid, S.M., Schaltegger, U., Krenn, E., Frank, W., Fügenschuh, B., 2010. Evolution of the Adria-Europe plate boundary in the northern Dinarides: From continent-continent collision to back-arc extension: ADRIA-EUROPE PLATE BOUNDARY, DINARIDES. Tectonics 29, n/a-n/a. https://doi.org/10.1029/2010TC002668

Valkaniotis, S., Papathanassiou, G., Ganas, A., Evagellos Kremastas, Caputo, R., 2021. Preliminary report of liquefaction phenomena triggered by the March 2021 earthquakes in Central Thessaly, Greece. Zenodo. https://doi.org/10.5281/ZENODO.4608365

Villani, F., Civico, R., Pucci, S., Pizzimenti, L., Nappi, R., De Martini, P.M., Villani, F., Civico, R., Pucci, S., Pizzimenti, L., Nappi, R., De Martini, P.M., Agosta, F., Alessio, G., Alfonsi, L., Amanti, M., Amoroso, S., Aringoli, D., Auciello, E., Azzaro, R., Baize, S., Bello, S., Benedetti, L., Bertagnini, A., Binda, G., Bisson, M., Blumetti, A.M., Bonadeo, L., Boncio, P., Bornemann, P., Branca, S.,

Braun, T., Brozzetti, F., Brunori, C.A., Burrato, P., Caciagli, M., Campobasso, C., Carafa, M., Cinti, F.R., Cirillo, D., Comerci, V., Cucci, L., De Ritis, R., Deiana, G., Del Carlo, P., Del Rio, L., Delorme, A., Di Manna, P., Di Naccio, D., Falconi, L., Falcucci, E., Farabollini, P., Faure Walker, J.P., Ferrarini, F., Ferrario, M.F., Ferry, M., Feuillet, N., Fleury, J., Fracassi, U., Frigerio, C., Galluzzo, F., Gambillara, R., Gaudiosi, G., Goodall, H., Gori, S., Gregory, L.C., Guerrieri, L., Hailemikael, S., Hollingsworth, J., Iezzi, F., Invernizzi, C., Jablonská, D., Jacques, E., Jomard, H., Kastelic, V., Klinger, Y., Lavecchia, G., Leclerc, F., Liberi, F., Lisi, A., Livio, F., Lo Sardo, L., Malet, J.P., Mariucci, M.T., Materazzi, M., Maubant, L., Mazzarini, F., McCaffrey, K.J.W., Michetti, A.M., Mildon, Z.K., Montone, P., Moro, M., Nave, R., Odin, M., Pace, B., Paggi, S., Pagliuca, N., Pambianchi, G., Pantosti, D., Patera, A., Pérouse, E., Pezzo, G., Piccardi, L., Pierantoni, P.P., Pignone, M., Pinzi, S., Pistolesi, E., Point, J., Pousse, L., Pozzi, A., Proposito, M., Puglisi, C., Puliti, I., Ricci, T., Ripamonti, L., Rizza, M., Roberts, G.P., Roncoroni, M., Sapia, V., Saroli, M., Sciarra, A., Scotti, O., Skupinski, G., Smedile, A., Soquet, A., Tarabusi, G., Tarquini, S., Terrana, S., Tesson, J., Tondi, E., Valentini, A., Vallone, R., Van der Woerd, J., Vannoli, P., Venuti, A., Vittori, E., Volatili, T., Wedmore, L.N.J., Wilkinson, M., Zambrano, M., 2018. A database of the coseismic effects following the 30 October 2016 Norcia earthquake in Central Italy. Scientific Data 5, 180049. https://doi.org/10.1038/sdata.2018.49

Weber, J., Vrabec, M., Pavlovčič-Prešeren, P., Dixon, T., Jiang, Y., Stopar, B., 2010. GPS-derived motion of the Adriatic microplate from Istria Peninsula and Po Plain sites, and geodynamic implications. Tectonophysics 483, 214–222. https://doi.org/10.1016/j.tecto.2009.09.001

Wells, D.L., Coppersmith, K.J., 1994. New empirical relationships among magnitude, rupture length, rupture width, rupture area, and surface displacement. Bulletin of the Seismological Society of America 84, 974–1002.

Xiong, W., Yu, P., Chen, W., Liu, G., Zhao, B., Nie, Z., Qiao, X., 2021. The 2020 Mw 6.4 Petrinja earthquake: A dextral event with large coseismic slip highlights a complex fault system in northwestern Croatia. Geophysical Journal International ggab440. https://doi.org/10.1093/gji/ggab440